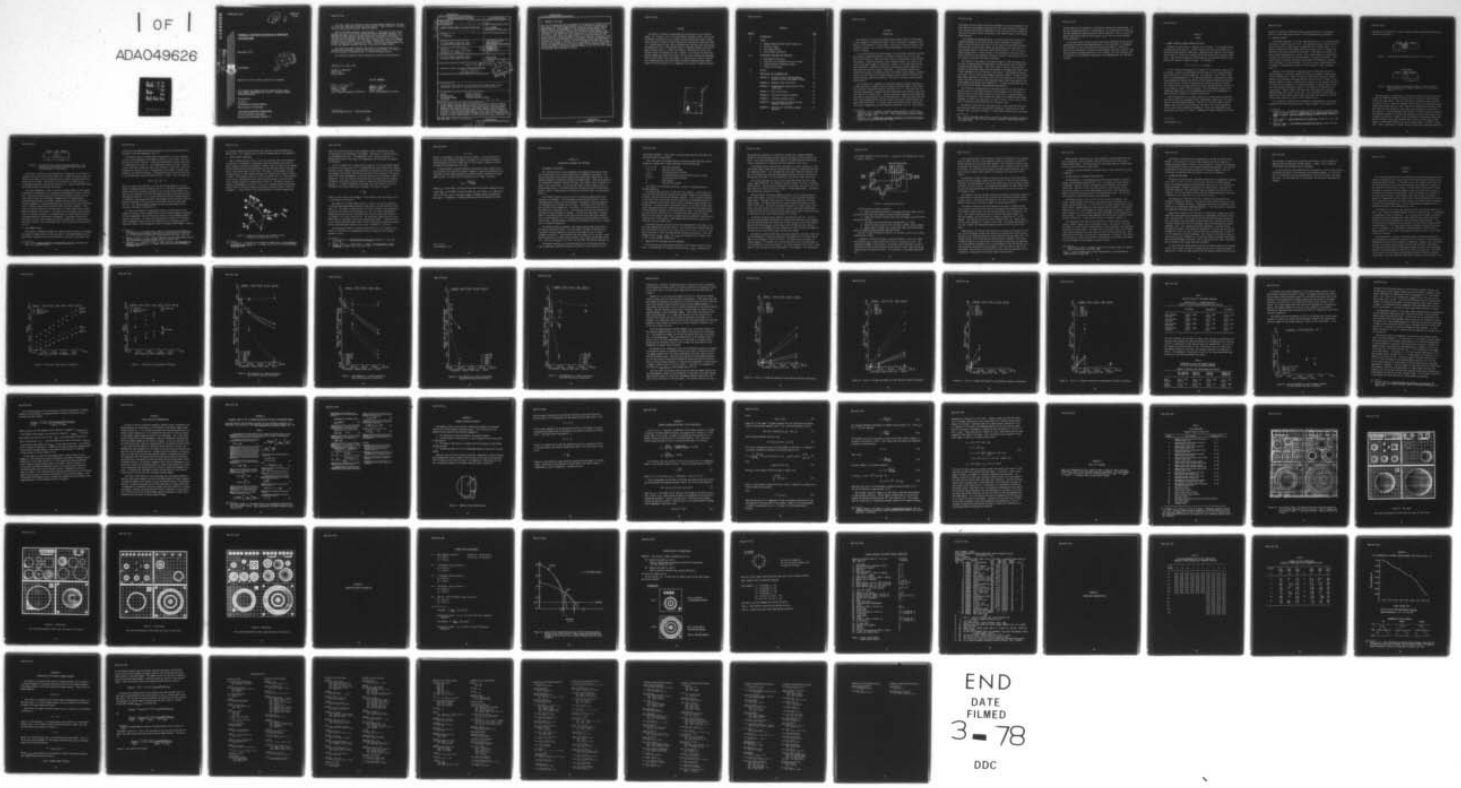
AD-A049 626 AIR FORCE WEAPONS LAB KIRTLAND AFB N MEX F/G 9/1
THERMAL NEUTRON DAMAGE IN BIPOLAR TRANSISTORS.(U)
DEC 77 T D STANLEY
UNCLASSIFIED AFWL-TR-77-168 NL

1 OF 1
ADA049626



END
DATE FILMED
3-78
DDC

AD A049626

DDC FILE COPY

AFWL-TR-77-168

12 2

AFWL-TR-
77-168

THERMAL NEUTRON DAMAGE IN BIPOLAR TRANSISTORS

December 1977

DDC
RECEIVED
FEB 3 1978
F

Final Report

Approved for public release; distribution unlimited.

This research was sponsored by the Defense Nuclear Agency under Subtask Z99QAXTB037, Work Unit 01, "Radiation Effects on Microelectronics."

Prepared for
Director
DEFENSE NUCLEAR AGENCY
Washington, DC 20305

AIR FORCE WEAPONS LABORATORY
Air Force Systems Command
Kirtland Air Force Base, NM 87117

0374

This final report was prepared by the Air Force Weapons Laboratory, Kirtland Air Force Base, New Mexico, under Job Order 88091132. Major Richard D. Chronister (ELP) was the Laboratory Project Officer-in-Charge.

When US Government drawings, specifications, or other data are used for any purpose other than a definitely related Government procurement operation, the Government thereby incurs no responsibility nor any obligation whatsoever, and the fact that the Government may have formulated, furnished, or in any way supplied the said drawings, specifications, or other data is not to be regarded by implication or otherwise as in any manner licensing the holder or any other person or corporation or conveying any rights or permission to manufacture, use, or sell any patented invention that may in any way be related thereto.

This report has been reviewed by the Office of Information (SUI) and is releasable to the National Technical Information Service (NTIS). At NTIS, it will be available to the general public, including foreign nations.

This technical report has been reviewed and is approved for publication.

Richard D. Chronister

RICHARD D. CHRONISTER
Major, USAF
Project Officer

FOR THE COMMANDER

Aaron B. Loggins

AARON B. LOGGINS
Lt Colonel, USAF
Chief, Transient Radiation Effects Br

Donald A. Dowler

DONALD A. DOWLER
Colonel, USAF
Chief, Electromagnetics Division

DO NOT RETURN THIS COPY. RETAIN OR DESTROY.

DNA PRINTING PLANT

UNCLASSIFIED

SECURITY CLASSIFICATION OF THIS PAGE (When Data Entered)

REPORT DOCUMENTATION PAGE

READ INSTRUCTIONS BEFORE COMPLETING FORM

1. REPORT NUMBER: AFWL-TR-77-168	2. GOVT ACCESSION NO.
3. RECIPIENT'S CATALOG NUMBER	
4. TITLE (and Subtitle): THERMAL NEUTRON DAMAGE IN BIPOLAR TRANSISTORS.	5. TYPE OF REPORT & PERIOD COVERED: Final Report.
	6. PERFORMING ORG. REPORT NUMBER
7. AUTHOR(s): T. D. Stanley	8. CONTRACT OR GRANT NUMBER(s)
9. PERFORMING ORGANIZATION NAME AND ADDRESS: Air Force Weapons Laboratory (ELP) Kirtland Air Force Base, NM 87117	10. PROGRAM ELEMENT, PROJECT, TASK AREA & WORK UNIT NUMBERS: 62601F/88091132 62704H/Subtask Z99QAXTB037/ Work Unit 01
11. CONTROLLING OFFICE NAME AND ADDRESS: Director Defense Nuclear Agency Washington, D.C. 20305	12. REPORT DATE: December 1977
	13. NUMBER OF PAGES: 78
14. MONITORING AGENCY NAME & ADDRESS (if different from Controlling Office): Air Force Weapons Laboratory (ELP) Kirtland Air Force Base, NM 87117	15. SECURITY CLASS. (of this report): UNCLASSIFIED
	15a. DECLASSIFICATION/DOWNGRADING SCHEDULE

16. DISTRIBUTION STATEMENT (of this Report)

88091 Z99QAXT

Approved for public release; distribution unlimited.

11 B037

DDC RECEIVED FEB 3 1978 F

17. DISTRIBUTION STATEMENT (of the abstract entered in Block 20, if different from Report)

18. SUPPLEMENTARY NOTES

This research was sponsored by the Defense Nuclear Agency under Subtask Z99QAXTB037, Work Unit 01, "Radiation Effects on Microelectronics."

19. KEY WORDS (Continue on reverse side if necessary and identify by block number)

Neutron
Thermal Neutron
Displacement Damage
Transistor
Bipolar Transistor
Radiation Effects
Transient Radiation Effects

20. ABSTRACT (Continue on reverse side if necessary and identify by block number)

An experimental test was made of the hypothesis that the source of thermal neutron damage in bipolar PNP transistors is the result of thermal neutron captures by the Boron-10 present in the emitter region of the transistors. Transistors were specifically made using three different ratios of Boron-10 to Boron-11 as the emitter dopant material, and in four different geometries. Forty-two of these specially made transistors were exposed to thermal neutron fluences as high as approximately 5 x 10^{15} neutrons per square centimeter. In

DD FORM 1 JAN 73 1473 EDITION OF 1 NOV 65 IS OBSOLETE

UNCLASSIFIED

SECURITY CLASSIFICATION OF THIS PAGE (When Data Entered)

013 150

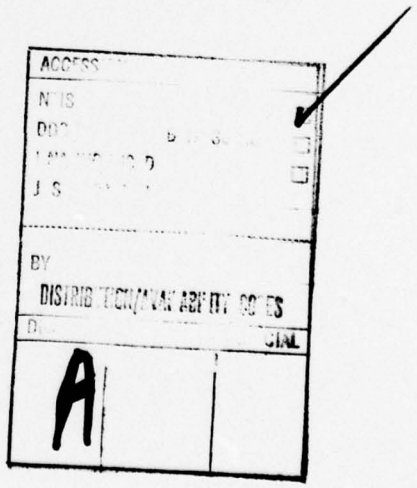
LB

20. ABSTRACT (continued)

each case the damage observed corresponded to the fraction of Boron-10 to total boron used as the emitter dopant material, thus confirming the hypothesized damage mechanism. The dependence of the collector current, thermal neutron fluence, and emitter-base geometry on the observed gain degradation also indicated that bulk damage is responsible for thermal neutron damage in PNP transistors. Some devices were also irradiated in a fast-neutron environment. Fast neutrons were found to be approximately 100 times more effective than thermal neutrons in producing damage in the devices that use a naturally occurring ratio of Boron-10 to Boron-11 in the emitter. Formulas were developed to calculate the fraction of lithium atoms and alpha particles generated in the emitter that do damage in the base, and to calculate the relative effectiveness of fast and thermal neutrons in producing damage in PNP transistors where the combined thickness of the emitter and base regions is less than the path length of a 0.88 MeV lithium nucleus in silicon.

PREFACE

The author is pleased to acknowledge the contributions of the following people: Dr. Patrick J. Vail, Air Force Weapons Laboratory (ELPT), who was the originator and sponsor for this project and who provided many helpful suggestions; Richard E. Anderson, Sandia Laboratories, who made the transistors used in a limited amount of time, and who answered many questions about the devices; the operations staff of the National Bureau of Standards Reactor, particularly Nathan Bickford and Dr. T. Raby; the Electronic Technology Division of the National Bureau of Standards for their interest in the project and their many helpful suggestions; Major Bruce Pierce, the Air Force Institute of Technology (AFIT) faculty advisor for this project; Dr. George John of the AFIT faculty, who provided essential help with several problems encountered; Major Robert Couch of the AFIT faculty for his suggestion to use Boron-11 doped transistors.



CONTENTS

Section		Page
I	INTRODUCTION	5
II	THEORY	8
	1. Damage Producing Thermal Neutron Reactions	8
	2. Transistor Theory	9
	3. Bulk Damage Effects	11
	4. Lattice Defect Production	13
III	EXPERIMENTAL EQUIPMENT AND PROCEDURE	16
	1. Experimental Transistors	16
	2. Transistor Test Equipment and Test Procedure	17
	3. National Bureau of Standards Reactor	21
	4. Irradiation Procedure	22
IV	RESULTS	24
V	CONCLUSIONS AND RECOMMENDATIONS	40
	APPENDIX A: A General Proof of the Degradation Equation for Bulk Displacement Damage	41
	APPENDIX B: Geometry Factor Calculation	43
	APPENDIX C: Thermal Neutron Reaction Rate in PNP Transistors	45
	APPENDIX D: NBS-2 Test Pattern	49
	APPENDIX E: Transistor Process Information	56
	APPENDIX F: Transistor Characteristics	63
	APPENDIX G: Flux Information on Thermal Column Pneumatic Tube Facility	66
	APPENDIX H: Derivation of the Relative Damage Equation	67

SECTION I

INTRODUCTION

The detonation of nuclear and thermonuclear weapons results in the release of large numbers of high-energy neutrons. When a transistor is exposed to fast neutrons, displacement of silicon atoms in the crystal lattice structure of the transistor results. As a result of these displacements, the gain of the transistor is reduced.

If in traveling from the nuclear weapon to an electronic system the neutrons pass through a moderating material like water or carbon, they will be slowed until their velocity is about the same as that of the molecules of the surrounding material. These slow neutrons, called thermal neutrons, are unable to do direct displacement damage in transistors. However, it has been observed that some transistors irradiated with thermal neutrons suffer damage comparable to that resulting from fast neutron irradiations. Since thermal neutrons have insufficient energy to do damage directly, the thermal neutron damage is hypothesized to be the result of an energy producing nuclear reaction induced by the thermal neutrons, specifically the (n,α) reaction in the boron used as emitter dopant material.

Itsu Arimura and C. Rosenberg of the Boeing Aerospace Company indicated in a paper published in December 1973 that they had observed damage in PNP transistors resulting from thermal neutron irradiation (ref. 1). They found that the relative effectiveness of thermal neutrons compared to fast neutrons varied from less than 10^{-3} to nearly unity. They discovered that thermal neutron damage was much less in NPN transistors than in PNP transistors. They also found that thin-base, high-frequency devices are more sensitive to thermal neutrons than wide-base, power transistors. In contrast, power transistors are more sensitive to fast neutron damage than are high-frequency transistors (ref. 2). Additionally,

---

1. Arimura, I. and C. Rosenberg, "Anomalous Damage Mechanism in PNP Silicon Transistors Due to Thermal Neutrons," IEEE Transactions on Nuclear Science, NS-20 6, December 1973.
2. Ricketts, L. W., Fundamentals of Nuclear Hardening of Electronic Equipment, Wiley-Interscience, Inc., New York, 1972.

the thermal neutron fluence and current dependence of the gain degradation indicated that bulk displacement damage was the most likely degradation mechanism. These findings led Arimura and Rosenberg to the conclusion that the damage was the result of thermal neutron absorption by the Boron-10 atoms in the emitter dopant material.

This hypothesized damage mechanism is consistent with what Arimura and Rosenberg observed and has been seen by several subsequent investigators. Namely, since PNP transistors have 10^2 to 10^4 more boron than NPN transistors, PNP transistors should suffer greater gain degradation when subjected to a given thermal neutron fluence than should NPN transistors. Also, since the doping concentration is usually higher in high-frequency transistors than in power transistors, high-frequency transistors should be more sensitive to thermal neutron irradiation than power transistors.

The fraction of the atoms in the emitter region of a PNP transistor that are boron is approximately one-thousandth, and the fraction that are Boron-10 is about two ten-thousandths. Also, only a small fraction of the particles produced in the emitter region would be expected to do damage which would result in gain degradation in the transistor's base region. Some tentative calculations by Dr. Vail of the Air Force Weapons Laboratory (AFWL), Kirtland Air Force Base (KAFB), New Mexico, indicated that as few as 20 reactions in the emitter region could have occurred for some reported fluence levels using typical transistor geometry and doping level (appendix C). It seems inconceivable that so few particles could produce observable gain degradation.*

The Electronics Phenomenology and Technology Branch of the AFWL needed to know the source of the observed thermal neutron damage in PNP transistors to develop a means of performing theoretical calculations of expected damage in radiation environments. They proposed the study of the thermal neutron damage mechanism in bipolar PNP transistors as a thesis topic at the Air Force Institute of Technology, Wright-Patterson Air Force Base, Ohio.

The approach chosen for the investigation was to have some PNP transistors made that were electrically and physically identical, differing only in the isotopic ratio of Boron-10 to Boron-11. These devices would then be irradiated

*Dr. P. Vail of the AFWL, KAFB, NM, has written an unpublished paper concerning the calculation of reaction rate of neutrons absorbed in boron doped transistors, April 1976.

and the observed gain degradation correlated to the Boron-10 concentration. If the gain degradation observed is proportional to the concentration of Boron-10, then the hypothesized damage mechanism would be supported. Also, by having the devices specifically made for this purpose, control over the device geometry would be possible.

In the next section the basic theory required to understand and analyze the hypothesized thermal neutron damage mechanism in PNP transistors is presented. Also included is a short description of transistor operation. Section III describes the transistors, transistor test equipment, and nuclear reactors used; the experimental procedure employed is also included. The final sections give the results of the experiment, conclusions, and recommendations for additional research.

SECTION II

THEORY

1. DAMAGE PRODUCING THERMAL NEUTRON REACTIONS

Naturally occuring boron is composed of two isotopes: 19.78 percent Boron-10 and 80.22 percent Boron-11. Boron-10 atoms have a very high probability of capturing thermal neutrons (3840 barns) compared to most materials and in particular to Boron-11, which has a thermal neutron activation cross section of 0.005 barns. When a Boron-10 absorbs a thermal neutron, an exothermic reaction takes place which releases 2.78 MeV of energy. The reaction is

$$\beta^{10} + n \rightarrow Li^{7} + \alpha + 2.78 \text{ MeV}$$

In this reaction the probability of forming Li^7 in the ground state is only 6.4 percent. Usually an intermediate excited state of Li^7 is formed followed by the emission of a 0.48 MeV gamma ray. The remainder of the 2.78 MeV (2.30 MeV) is divided between the Li^7 and the alpha particle. Conservation of momentum considerations leads to the division of the remaining energy such that the alpha particle has 1.47 MeV of energy and the lithium ion receives 0.88 MeV. The lithium nucleus and alpha particle fly apart, dissipating their energies in a few microns of crystal lattice structure. The displacements caused by the lithium and alpha recoils are the hypothesized source of gain degradation in thermal neutron irradiation of bipolar transistors.*

Since the absorption of a thermal neutron by a silicon atom can transmute the silicon atom into a phosphorus atom, transmutation doping has to be considered as a possible damage mechanism. However, silicon has a thermal neutron capture cross section of only 0.09 barns; and out of 100 neutron captures in silicon, only 4 are transmuted to phosphorus. Also, the transmutation takes place with a half life of 2.6 hours. Absorption of thermal neutrons by silicon

---

*See footnote, p. 6.

produces an average of 780 MeV of kinetic energy applied to a silicon atom (ref. 3). Thus, while not promising, silicon capture must be considered.

2. TRANSISTOR THEORY

The bipolar transistor is a current amplifying device. It is a three-region device and is usually made of silicon. The regions are made by doping the silicon with boron for a p-type region or phosphorus for an n-type region. In p regions the majority of the charge carriers are holes, while in n regions the majority of the charge carriers are electrons. A PNP transistor consists of two p regions separated by an n region. One p region doped to a concentration of about 10^{16} boron atoms per cubic centimeter is called the collector. The n region, which is doped to a concentration of about 10^{18} phosphorus atoms per cubic centimeter, is called the base. The final p region, called the emitter, is doped to a concentration of about 10^{20} boron atoms per cubic centimeter (ref. 4).

Because of the difference in majority carrier concentration across the region boundaries, diffusion currents will flow in an attempt to balance the carrier concentrations. These currents will continue to flow until internal potentials are developed that cause the net flow of carriers to cease. If an external potential source is supplied to the junction of two regions with polarity such that the formation of an internal potential is opposed, then current will flow through the potential source. This condition is referred to as a forward bias. Figure 1 shows a PNP transistor with forward bias potential applied between the emitter and the base. Since the emitter is more heavily doped than the base, most of the current flow across the junction is from the flow of holes from the p region to the n region (ref. 5).

If a potential is applied so as to enhance the development of an internal potential, the flow of charge carriers is almost stopped. This situation is

---

3. Cleland, J. W., "Transmutation Doping and Recoil Effects in Semiconductors Exposed to Thermal Neutrons," Proceedings of the International Enrico Fermi School of Physics, Radiation Damage in Solids, Academic Press, New York, 1962.
4. Brophy, James J., Basic Electronics for Scientists, McGraw Hill, Inc., New York, 1969.
5. McKelvey, John P., Solid State and Semiconductor Physics, Harper and Row, New York, 1966.

referred to as reverse bias. Figure 2 shows a reverse bias applied between the base and the collector.

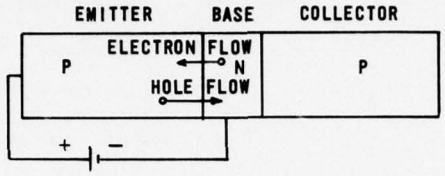


Figure 1. Forward Biased Emitted-Base Junction in PNP Transistor

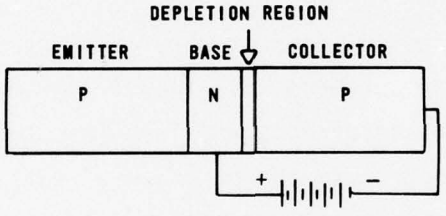


Figure 2. Reverse Biased Collector-Base Junction in PNP Transistor: Only the Few Carriers Thermally Generated in the Depletion Region Will Flow.

The base region in transistors is very thin (on the order of 0.5 microns), so that the diffusion length of minority carriers, holes, is longer than the width of the base region. When the transistor is biased for normal operation as shown in figure 3, holes are injected into the base region across the forward biased emitter base junction. Most of the holes diffuse right through the thin base region and are collected in the reverse bias potential of the collector-base junction. Since the collector-base junction is reverse biased, increasing the potential between the collector and the base will have little effect on the collector current flow. However, since the forward bias potential between the emitter and base controls the diffusion flow of holes into the base, a small change in emitter-base potential can cause a large change in collector current flow. Thus, a power gain in signals can be achieved using transistor amplifiers.

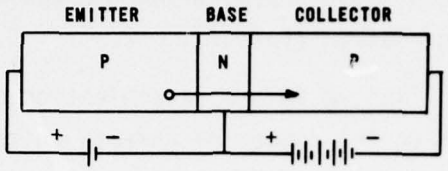


Figure 3. The PNP Transistor Biased for Normal Operation: Holes Generated in the Emitter Diffuse Through the Base and Are Accumulated in the Collector.

The DC gain, a measure of relative merit of a transistor, is the ratio of collector current flow to the base current flow. Ideally the base current flow should be very small, giving a large gain, but in actual practice the DC gain ranges from 20 to 1000. The DC gain is also referred to as Beta and H_{FE}. To be completely specified, the gain must be given for a specific collector current and voltage between the collector and emitter.

Since gain degradation is one of the most important effects of the neutron irradiation of transistors, it is important to understand the origin of the DC gain. There are several sources of base current including injection of electrons from the base into the emitter, leakage across the reverse biased collector-based junction, and surface currents from the emitter to the base. The main component is usually recombination of a portion of the holes with electrons in the base region before they can diffuse into the collector. Since holes are minority carriers in the base region, it seems likely that the holes would all combine with electrons. This does not occur, however, since recombination of electrons and holes is forbidden except at lattice defect sites due to quantum mechanical conservation requirements. These defect sites may be impurities or energy level changes resulting from vacancies or interstitials in the crystal lattice. Many such defects exist in even the best silicon crystals (ref. 6).

3. BULK DAMAGE EFFECTS

Fast-neutron irradiation degrades the transistor gain directly by increasing the number of lattice defects in the base region. Even though defects are produced evenly throughout the transistor material, only those in the base region

6. Larin, Frank, Radiation Effects in Semiconductor Devices, John Wiley and Sons, Inc., New York, 1968.

(and the two thin-depletion regions separating the base from the emitter and collector) cause gain degradation (ref. 7).

The minority carrier lifetime before recombination of a hole in N-doped silicon is thus dependent on the number of defects in the silicon. One over the minority carrier lifetime is called the recombination rate per carrier and is symbolized by the letter R. The recombination rate per carrier is proportional to the base current and, hence, the reciprocal of the gain. Also, the recombination rate per carrier is proportional to the number of defects and, therefore, the radiation exposure. Recombination rate per carrier is the sum of the recombination rates of different origins. Hence, it can be shown that

$$\Delta(1/\beta) = \frac{1}{\beta_f} - \frac{1}{\beta_i} = C\Phi$$

where β_f is gain after exposure, β_i is the gain before exposure, Φ is the fluence of damage producing radiations, and C is a constant of proportionality. Another form of this equation, referred to as the bulk damage equation, has been used for many years to predict the expected change in gain resulting from fast-neutrons exposure. The C, usually called the radiation damage constant, is dependent on the energy and type of displacement causing radiation, and the physical properties of the transistor, most notably the base transit time (ref. 8). The radiation damage constant (C) has also been shown to be a function of collector current (ref. 9).

As long as the number of recombination centers is proportional to the fluence of radiation, and no other effect (such as surface leakage or mechanical failure) predominates and significant gain remains, the bulk damage equation should be applicable. As long as the concentration of Boron-10 is not appreciably decreased by thermal neutron irradiation, the bulk damage equation is expected to apply to the hypothesized source of thermal neutron damage. However,

---

7. Donovan, R. P., J. R. Hauser and M. Simon, "A Survey of the Vulnerability of Contemporary Semiconductor Components to Nuclear Radiation," AFAL-TR-74-61, Air Force Avionics Laboratory, Wright-Patterson AFB, Ohio, June 1974.

8. Ramsey, C. and Dr. P. Vail, "Current Dependence of the Neutron Damage Factor," IEEE Transactions on Nuclear Science, NS-17 6, December 1970.

9. Crawford, J. H., "Radiation Effects in Ionic Crystals," The Interaction of Radiation with Solids, ed., R. Stumae, North Holland Publishing Company, Amsterdam, 1964.

the radiation damage constant would be very sensitive to device geometry and doping levels. For a general proof of the bulk damage equation, see appendix A.

4. LATTICE DEFECT PRODUCTION

When a charged particle moves in a lattice structure, most of the energy of the particle is dissipated in interactions with the electrons of the lattice atoms, causing no lattice displacements. However, when the energy of the charged particle falls below the threshold energy for the particular lattice structure, atomic interactions begin to take place. The result is displacement of atoms leaving vacancies in some lattice positions and interstitials (excess of atoms) in others. The threshold energy in silicon is 145 keV (ref. 9). Atoms displaced by the initial charged particle may have sufficient energy to displace other atoms, thereby producing a cascade effect (figure 4). The energy required to produce a displacement in silicon in 12.9 eV, so a charged particle with energy greater than the threshold energy could produce a maximum of about 11,000 displacements. A large portion of the atoms displaced in radiation damage moves

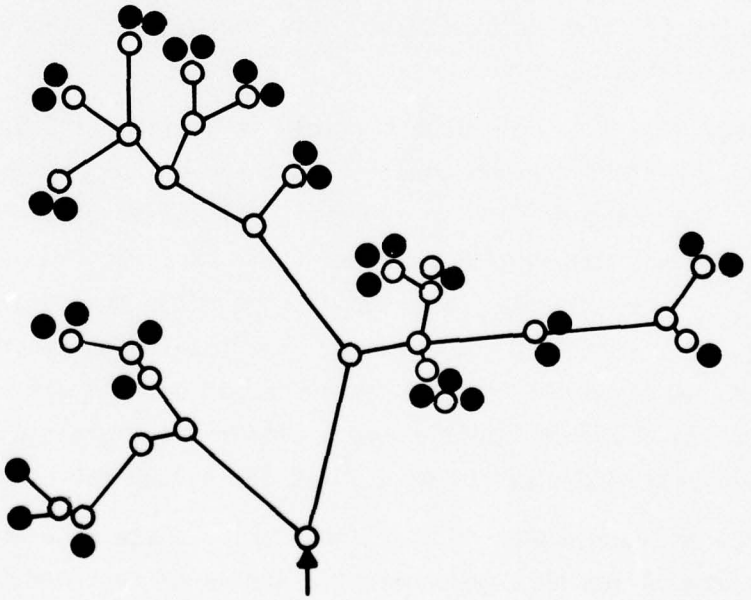


Figure 4. Example of a Crystal Lattice Damage Cascade:
O Vacancy, ● Interstitials (ref. 10)

10. Leibfried, G., "Introduction into Radiation Damage Theory," The Interaction of Radiation with Solids, ed., R. Stumae, North Holland Publishing Company, Amsterdam, 1964.

back into lattice positions or form complexes (such as divacancies) within milliseconds of the occurrence of the damage. The result is a partial healing of the damaged transistor. This phenomenon, which is called annealing, is temperature sensitive; the higher the temperature, the more rapid and complete the annealing.

If it is assumed that a charged particle does all of its displacement damage at the end of its path, and if it is assumed that the path length of the charged particle is small compared to the surface area of the device so that semi-infinite slab geometry can be used, then the portion of particles produced in the emitter region that cause displacements in the base region can be calculated as shown in appendix B. Also, the range of the particle must be greater than the combined thickness of the emitter and base regions to apply the relationship derived in appendix B. If these assumptions can be made, then the fraction of particles produced in the emitter region that do damage in the base is given by

$$G = \frac{h}{2R}$$

where G is the fraction doing damage, *h is the width of the base region*, and R is the range of the particle.

The range of a 1.47 MeV alpha particle in silicon is 5.5 μm as determined by applying the Bragg-Kleeman equation to the range of an alpha particle in air (ref. 11). The range of lithium nuclei in silicon is given in ion implantation literature for various initial energies (ref. 12). By linear interpolation between the 300 keV and the 1 MeV ranges, one finds the total path length for a 0.88 MeV Li in silicon to be 3.12 μm. The total path length should, for this application, be corrected to give the projected path length. A correction factor of 0.96 was obtained, again using a linear interpolation between data points, giving a projected path length of 3.00 μm for a 0.88 MeV Li in silicon.

To calculate the number of reactions taking place in a unit volume as the result of irradiation by a monoenergetic source of neutrons, the following equation is used

---

11. Price, William J., Nuclear Radiation Detection, McGraw-Hill, Inc., New York, 1964.
12. Davies, John A., L. Erikson and J. W. Mayer, Ion Implantation in Semiconductors, Academic Press, New York, 1970.

$$R = \sigma N \Phi$$

where R is the number of reactions per unit volume, σ is the reaction cross section for the reaction and energy of interest, N is the number of atoms of reacting material per unit volume, and Φ is the fluence of neutrons to which the material was exposed per unit area.

For distributions of neutron energies, the problem is more complex since cross sections are functions of energy. Appendix C shows the derivation of the reactions per unit volume resulting from thermal neutron irradiation of boron doped silicon. For this case the reaction per unit volume is given by

$$R_{\alpha,Li} = \frac{N_{B10}\ \sigma_0\ \Phi}{1.128}$$

where $R_{\sigma,Li}$ is the number of alpha particles and lithium atoms produced per unit volume, N_{B10} is the number of Boron-10 atoms per unit volume, σ_o is 3840 barns = 3.84×10^{-21} cm^2, and Φ is the total number of thermal neutrons incident per unit area.* *In appendix C a sample calculation using this equation is given.*

*See footnote, p. 6.

SECTION III

EXPERIMENTAL EQUIPMENT AND PROCEDURE

1. EXPERIMENTAL TRANSISTORS

The transistors used in this experiment were produced at the Device Design and Processing Division of Sandia Laboratories, Albuquerque, New Mexico. The devices were made in an Extrion Automated Ion-implantation Chamber using a test pattern produced by the National Bureau of Standards (NBS). Since the process of ion-implantation separates isotopes by weight, the isotopic ratio of Boron-10 to Boron-11 was controllable. The devices were made in three isotopic ratios of emitter-dopant atoms: 100 percent Boron-10, 20 percent Boron-10 and 80 percent Boron-11 (which is approximately the naturally occurring ratio), and 100 percent Boron-11.

Two different times were used to drive in the emitter dopant atoms after they were ion implanted. Since the base had previously been driven in for an extended period of time, only the thickness of the emitter region was appreciably affected by the different drive-in times. Consequently, the transistors were available in two geometries: (a) emitter 1.1 μm and the base 0.5 μm, and (b) emitter 0.9 μm and base 0.7 μm. The narrow-base devices are referred to as high-gain and the wide-base as low-gain. For both cases the number of dopant atoms in the emitter region was the same since the boron atoms were implanted with a surface density of 5×10^{15} boron atoms per square centimeter of emitter surface area. Complete process information with doping profiles and pin arrangement is included in appendix D.

The National Bureau of Standards test pattern used was NBS-2 described in NBS Special Publication 400-6. This test pattern includes 20 different test structures including capacitors, resistors, and diodes as well as several different transistors. The structures that were bonded out for use were a small emitter transistor, an emitter sheet resistor, and a large area tetrode transistor. These are structures 7, 15, and 19 on the NBS-2 test pattern (appendix E).

The tetrode transistor has two base contacts, one at the center and one at the circumference, enabling the device to be used as a base resistor or as a

large area transistor. Since there is no passivation mask with the NBS-2 set, the devices were not passivated.

Thus, there were 12 different types of transistors made which were distinguished by a number and a letter according to the following code:

2, 6, or 10	Low Gain (wide base)
4, 8, or 12	High Gain (narrow base)
2 or 4	100 percent Boron-11 emitter
6 or 8	20 percent Boron-10 and 80 percent Boron-11 emitter
10 or 12	100 percent Boron-10 emitter
A	Small emitter
B	Large emitter tetrode

For example, a 2B transistor would be a low-gain, 100 percent Boron-11 tetrode transistor.

The devices were supplied in eight-lead TO-5 packages. A field plate contact over the collector-base junction was included in addition to the emitter, collector, and base (two for the tetrode) contacts. Since a changing potential on the field plate could affect the device operation and radiation sensitivity, it was soldered to the collector lead so that a consistent potential would be maintained. The leads going to the emitter resistor in the small emitter transistor package were bent 90° forward and spaced so that they could make contact with four adjacent contacts in an eight-lead TO-5 socket. The transistor leads were bent so that they would fit in a standard four-lead transistor socket. Devices of each specific type were assigned consecutive numbers to enable unique identification of each device. These numbers were painted on the top of the transistor case with enamel paint.

The three transistors of each variety were characterized on the AFWL's Fairchild 600 Computerized Transistor Testor. The characteristics measured were the gain at collector currents of 0.01, 0.02, 0.05, 0.1, 0.2, 0.5, 1, 2, 5, 10, and 20 milliamps with 5 volts maintained between collector and emitter. Also, the leakage currents $I_{(CBO)}$, $I_{(EBO)}$, and $I_{(CEO)}$ were measured with voltages of 10, 3, and 10 volts applied, respectively.

2. TRANSISTOR TEST EQUIPMENT AND TEST PROCEDURE

The 72 devices were characterized before and after thermal neutron irradiations. The characteristics measured included DC gain, $I_{(EBO)}$, capacitance of

the emitter-base junction as a function of reverse bias voltage, breakdown voltage of the emitter-base junction, emitter resistance, and base sheet resistance. Also, scope photographs were taken of the common emitter characteristic curves as displayed on a Tektronik Type 575 Transistor Curve Tracer.

The equipment used to measure gain consisted of a current regulator, a regulated power supply, three digital voltage-current meters, a transistor test box, and connecting cables. This equipment was also used to measure saturation voltage, the voltage drop across the emitter-base junction, the base resistance for the tetrode transistors, and the resistance of the emitter sheet resistances.

The current regulator was built using a Kepco Operational Amplifier power supply, model OPS1C0-2TA. It supplied a constant current for use as a collector current source. The current was selectable in two ranges, from 0.25 to 10 milliamps, and was set with a precision, 10-turn, 1-kilohm potentiometer. The compliance voltage was limited to 15 volts.

The base current source was formed by placing a high resistance (approximately 100 kilohms) in series with the output of a well-regulated laboratory power supply. The power supply used was a Trygon Electronics Dual Lab Power Supply, DL40-1. The power supply had an output voltage continuously variable from 0 to 40 volts. The series resistance consisted of a fixed, 2-watt, wirewound, 10-kilohm resistor and a precision, 10-turn, 500-kilohm potentiometer. By adjusting the series resistance and the power supply output voltage, the base current could be set from a few microamps to 4 milliamps.

The series resistances were housed in the transistor test box. This box also contained switches which enable the voltage being monitored to be switched from the voltage between the emitter and collector $\left(V_{CE}\right)$ to the voltage between the base and emitter $\left(V_{BE}\right)$ or the voltage across the emitter sheet resistor. The test box also contained the jacks necessary to attach the other equipment to the transistor or the emitter sheet resistor being tested.

The digital voltage-current meters used were Honeywell's Digitest, Model 333, Digital Multimeters. These are three-digit instruments with full-scale ranges down to 99.9 microamps or 99.9 millivolts. The maximum error of reading on current ranges is 1.5 percent plus or minus one digit, and on voltage ranges it is 0.5 percent plus or minus one digit. The input impedance on the 10-volt scale (which is the one used for gain measurements) is 100 megohms. The voltage drop

for current readings is 100 millivolts. A diagram of the complete test circuit is given in figure 5.

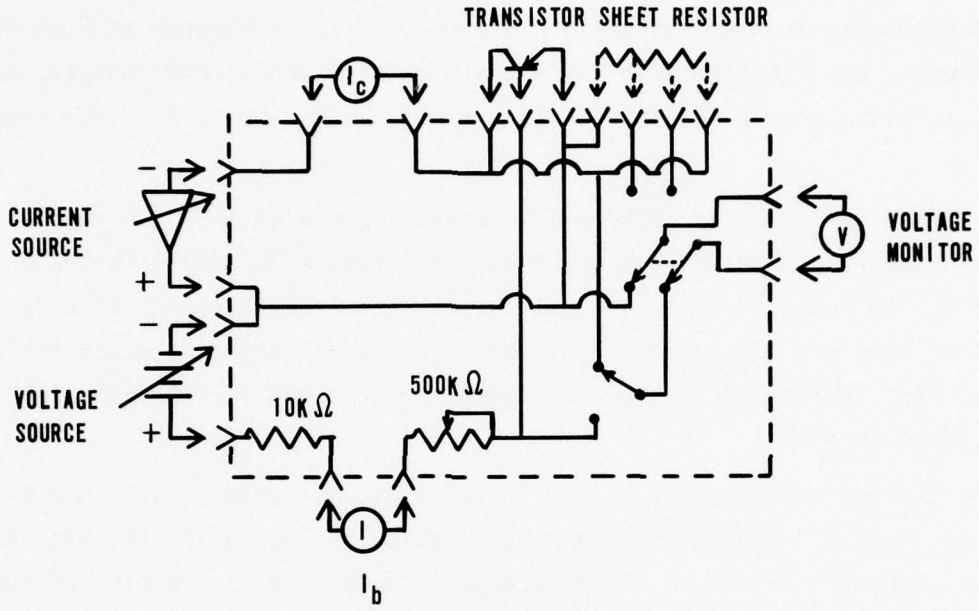


Figure 5. Transistor Test Circuit

Transistor gain is tested as follows:

a. After placing the transistor in the transistor test socket, turn up the base current until the reading is several hundred microamps.

b. Adjust the collector current source for the highest current at which the gain is desired.

c. Turn down the base current until the desired V_{CE} is read.

d. Record the base current for the collector, current, and V_{CE} chosen.

e. Repeat steps b through d for successively lower collector currents until all desired operating points have been tested.

The gain is then calculated by dividing the collector current by the corresponding base current.

To measure a saturation voltage, a similar procedure is used; only rather than setting a V_{CE}, a base current which results in saturation is set. The saturation voltage is read directly. The emitter sheet resistance is read by setting the collector current source for the desired current, then reading the voltage across the emitter resistor. The resistance is calculated using Ohm's law.

It was observed that if the collector current is maintained over an extended period of time, the gain of the transistor appears to increase as a result of thermal drifting due to internal ohmic heating. The drifting was found to cause an apparent gain increase of up to 8.5 percent after 5 minutes at 6 mA of collector current. By starting with the highest current and working quickly down to lower currents, thermal drift effects are minimized since total test time is reduced.

An additional problem, observed in measuring the gain of the large emitter devices, was large leakage current flow (as large as 0.7 mA) with the base open. Therefore, gain measurements for the large emitter devices for collector currents less than 1 mA were not used. The remaining measurements for these devices must be used with the knowledge that the indicated gain may be high as a result of the leakage current.

The leakage of the base emitter junction was measured since gamma irradiation of transistors can degrade the gain by drastically increasing the base emitter leakage current. The cause of the damage in this case is trapping of ions produced in the surface of the device above the emitter-base junction.

The method of measuring the base leakage was to apply a constant reverse bias voltage to the emitter-base junction and measure the leakage current flow. The constant voltage source used was a mercury battery with an output of 1.35 volts. The current was measured using a Keithley Instruments, Model 153, Microvolt-ammeter, which was capable of reading currents from 10^{-1} to 10^{-11} amperes. The accuracy was plus or minus 4 percent on the 10^{-11} ampere scale, with an input impedance of 1 megohm on that range. The battery was housed in a box with a switch that removed the battery from the circuit for zeroing the meter.

Capacitance of the emitter-base junction as a function of reverse bias voltage, and the breakdown voltage, and voltage of the emitter-base junction were measured using a Boonton Electronics Direct Capacitance Bridge, Model 750. The voltage applied to the transistor was monitored with a Honeywell three-digit Voltmeter, Model 33, and the current flow through the transistor was monitored with an ME-70A/PSM-6 Standard US Air Force Multimeter on the 100 microamp scale. The information obtained with this equipment, while not directly used in the experiment, helps to verify the similarity of the electrical properties of the transistors, irrespective of the boron isotope used for doping.

Common emitter characteristics of the transistors were recorded before and after irradiation, using a Tektronic Type 575 Transistor Curve Tracer and a Polaroid Scope Camera. These characteristic curves were taken as a backup data source and were not used as a data source.

A summary of the preirradiation characteristics of the transistors is given in appendix F.

3. NATIONAL BUREAU OF STANDARDS (NBS) REACTOR

The NBS Reactor is a D_2O moderated and cooled reactor located in the NBS complex at Gaithersburg, Maryland (ref. 13). It operates at a power output of 10 megawatts (thermal) using 5.4 kilograms of fuel enriched to 93 percent Uranium 235. The fuel is split into two sections so that fissions are not taking place directly in front of experimental facilities, thus reducing the gamma ray and fast neutron exposures in the experimental areas. The facility was designed for high thermal neutron flux experiments.

The thermal column is a 54- by 52- by 37-inch block of graphite. The thermal column pneumatic tube facility was used to expose the transistors to thermal neutron irradiation. In this facility the copper cadmium ratio is 3415, which implies a thermal neutron to fast neutron ratio of 30,000.* The absolute neutron flux is 1.6×10^{11} neutrons per square centimeter per second, so that total fluences of 5×10^{15} neutrons per square centimeter can be accumulated in about 8 hours. The thermal column pneumatic tube facility was carefully characterized in June 1971. A copy of this finding is included in appendix G.

The transistors were sent into the reactor--in a small plastic container called a rabbit--along a series of pneumatic tubes. The length of time that the rabbit is in the reactor is determined by a timer installed in the pneumatic tube facility control panel. The timer used in the control panel can be chosen from several different full-scale ranges to allow more accurate setting. When setting near full-scale, the accuracy is approximately ± 2 percent. The rabbits are returned to a lead pig so that their radioactivity can be monitored without excessive exposure of the operator to gamma radiation.

---

13. "NBS Reactor," Public Information Sheet on the National Bureau of Standards Reactor, Gaithersburg, Maryland, 1969.

*Raby, T., private communication on the characteristics of the NBS Reactor Thermal Column, 22 June 1976.

Fast-neutron irradiations were accomplished in the SPR-II Sandia Pulsed Reactor. This reactor is a bare critical assembly so that the spectrum of neutron energies produced is nearly a fission spectrum. Using sulfur dosimetry, a 1-MeV-equivalent fluence for the neutron exposure was obtained. The relative effectiveness of fast and thermal neutrons in producing damage in the test transistors was obtained using the results of the fast irradiations.

4. IRRADIATION PROCEDURE

One device of each type was irradiated successively to accumulative fluences of 5×10^{11}, 5×10^{12}, 5×10^{13}, and 2×10^{14}, and all but the 100 percent Boron-10 and 20 percent Boron-10 large-emitter devices to 5×10^{14} neutrons per square centimeter. Between irradiations, the common emitter characteristic curves were observed. No significant change was detected for the first two fluences. For the last three fluences, gain and leakage measurements were made in addition to the characteristic curves that were taken.

The temperature of the devices during irradiation was monitored using Tempilable Temperature Monitors. The range covered by these monitors was 130° F to 160° F in 10-degree increments. Temperature monitoring was important, since annealing is a temperature dependent phenomenon. Also, the times of irradiation and subsequent measurement were recorded.

Based on the finding of the first set of irradiations, fluences were calculated that would produce gain degradations of approximately 20 percent, 40 percent, and 60 percent. Two of each of the small-emitter high-gain transistors were irradiated to the calculated fluences except for all the Boron-11 devices. The upper fluence limit for this experiment, set by the NBS Radiation Hazards Committee, was 5×10^{15} neutrons per square centimeter. Since the fluence calculated to produce a 20 percent gain degradation in all the Boron-11 devices exceeded this limit, only two of these devices were irradiated to a fluence of 5×10^{15} neutrons per square centimeter. One of each of the remaining types of transistors was also irradiated to a fluence calculated to produce a gain degradation of approximately 60 percent. Due to time constraints, these irradiations were performed by NBS reactor operations personnel.

To insure that the damage observed was due to thermal neutrons and not gamma rays or fast neutrons, one device of each type was to be irradiated wrapped in cadmium foil. Since the cadmium would block out thermal neutrons while allowing

fast neutrons and gamma rays to penetrate the devices, any gain degradation observed would not be due to thermal neutrons. However, due to technical difficulties this experiment was not performed.

To insure that no stray potentials were developed as a result of the ionizing radiations, the leads of the transistors were shorted together. For the first sets of irradiations, this was accomplished by inserting the leads into conductive foam. For the second set of irradiations, the transistor leads were bent together.

SECTION IV

RESULTS

The initial characteristics of the devices confirm that they are electrically similar, regardless of the isotopic ratio of Boron-10 to Boron-11 atoms used as the emitter dopant material. In figures 6 and 7, the average initial gains (of the three transistors of each type characterized) are plotted as a function of the logarithm of the collector current. The deviations (of the gains of three transistors in each set from the average for the set) varied from 4 percent to 12 percent for the small emitter devices, and from 5 percent to 17 percent for the large emitter devices. These graphs, taken from the data presented in appendix F, demonstrate that the initial gains of the transistors, which differ only in the ratio of Boron-10 to Boron-11 used as the emitter dopant, correspond to within one standard deviation. The gain measurements correspond within 1.5 standard deviation to those obtained by Dr. Vail.

The fraction of the initial gain remaining (after each thermal neutron irradiation as a function of thermal neutron fluence for the first set of irradiations) is presented in figures 8 through 11. As is shown on these graphs, the 100 percent Boron-10 devices degraded with roughly one-fifth the fluence required to produce a similar gain degradation in the 20 percent Boron-10 devices. Also, no significant gain degradation was observed in the all-Boron-11 devices at the maximum fluence (5×10^{14} neutrons per square centimeter) achieved during this set of irradiations. The uncertainty in the measurements of gain, which is about 5 percent, is the source of the apparent increase in gain in some of the all-Boron-11 devices.

The large-emitter, low-gain, 100 percent Boron-11 transistor appeared to have suffered a gain degradation after its first irradiation, with no additional degradation occurring for the remaining irradiations. However, since the characteristic curve photos show no change from the preirradiation to the maximum irradiation, and since the 2-mA measurement showed no change, it was concluded that the initial measurement of the gain for this device was high. The source of the high initial gain reading was probably thermal drift due to a several minute delay in measuring the gain after applying power to the transistor. The

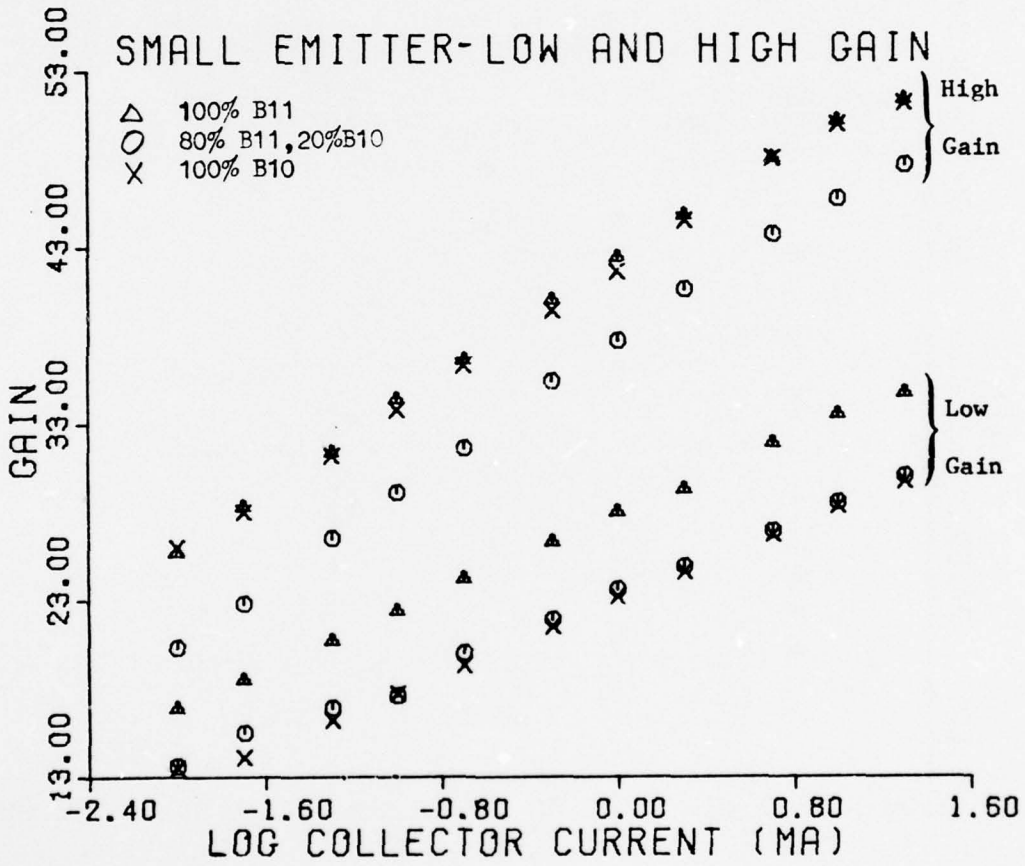


Figure 6. Initial Gain, Small-Emitter Transistors

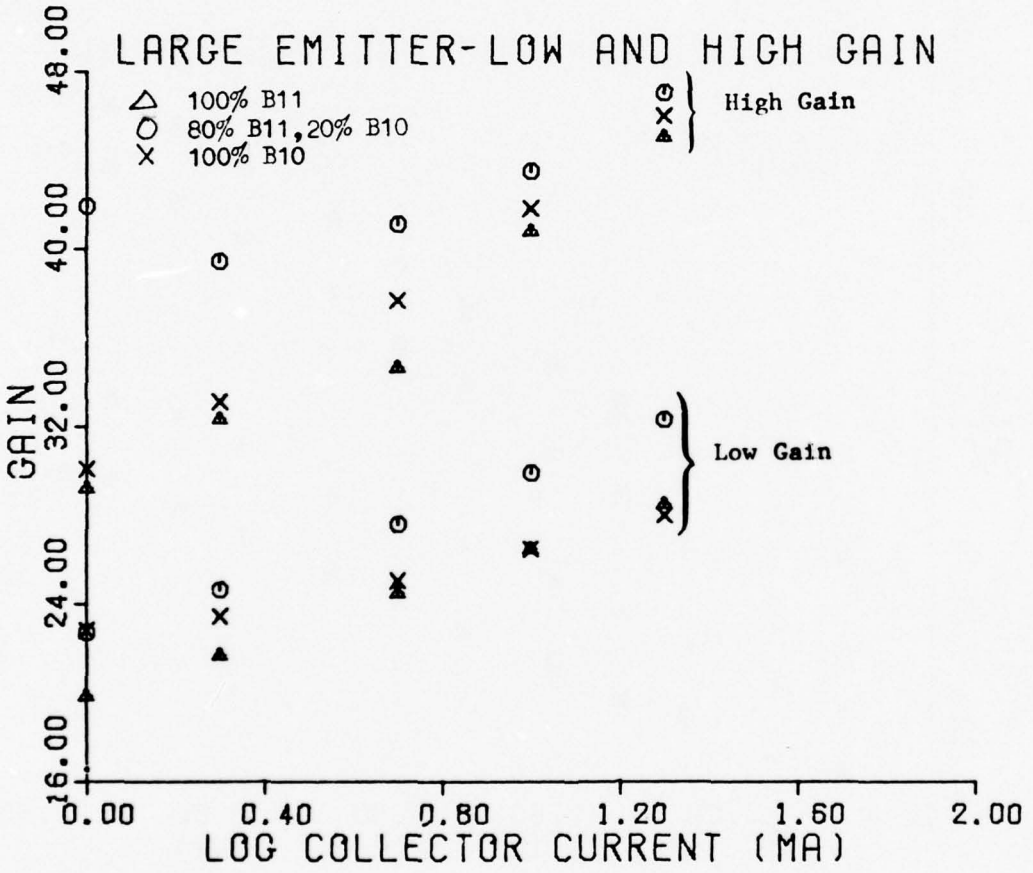


Figure 7. Initial Gain, Large-Emitter Transistors

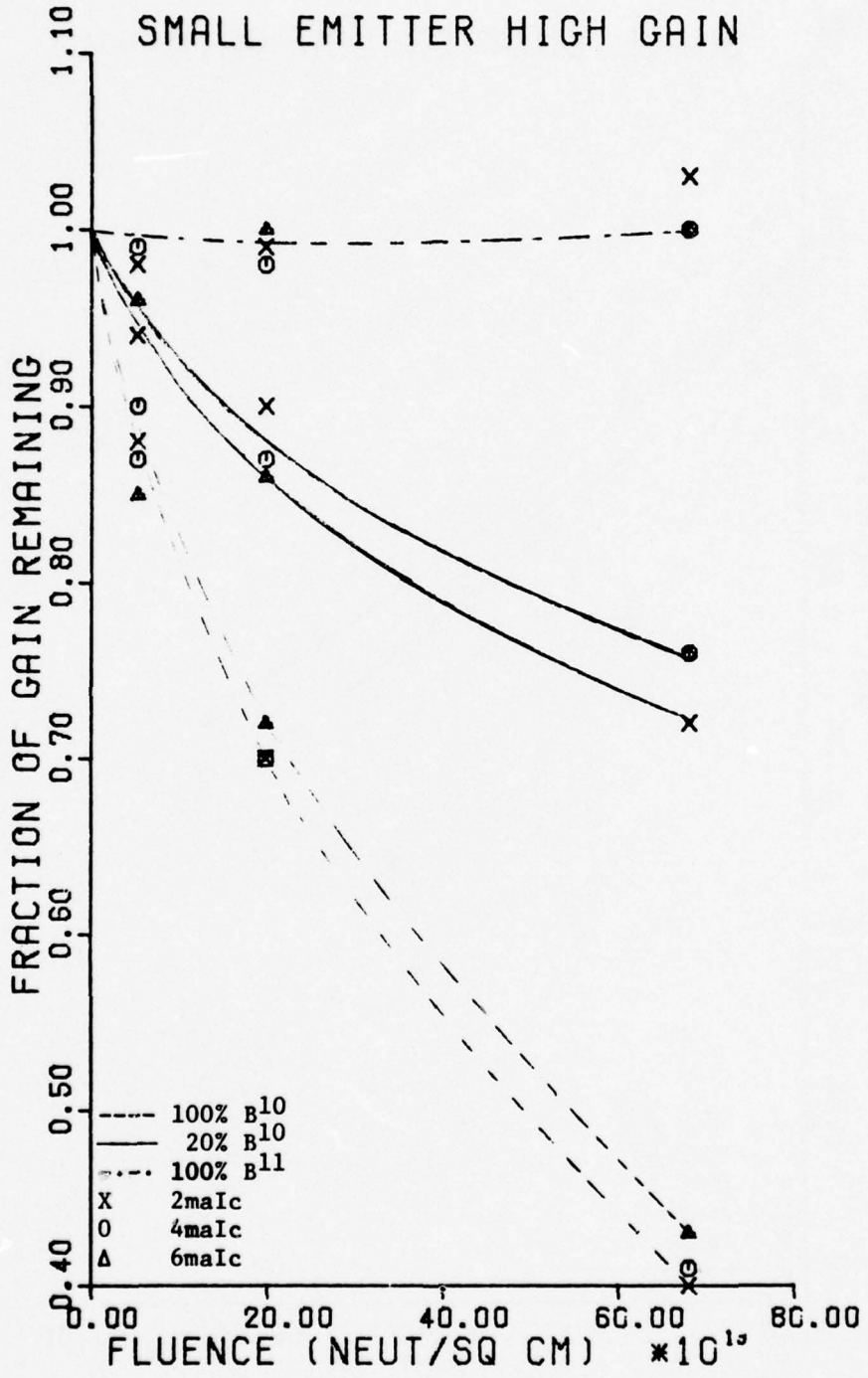


Figure 8. Gain Remaining vs. Fluence and Doping; Small-Emitter High-Gain Transistors

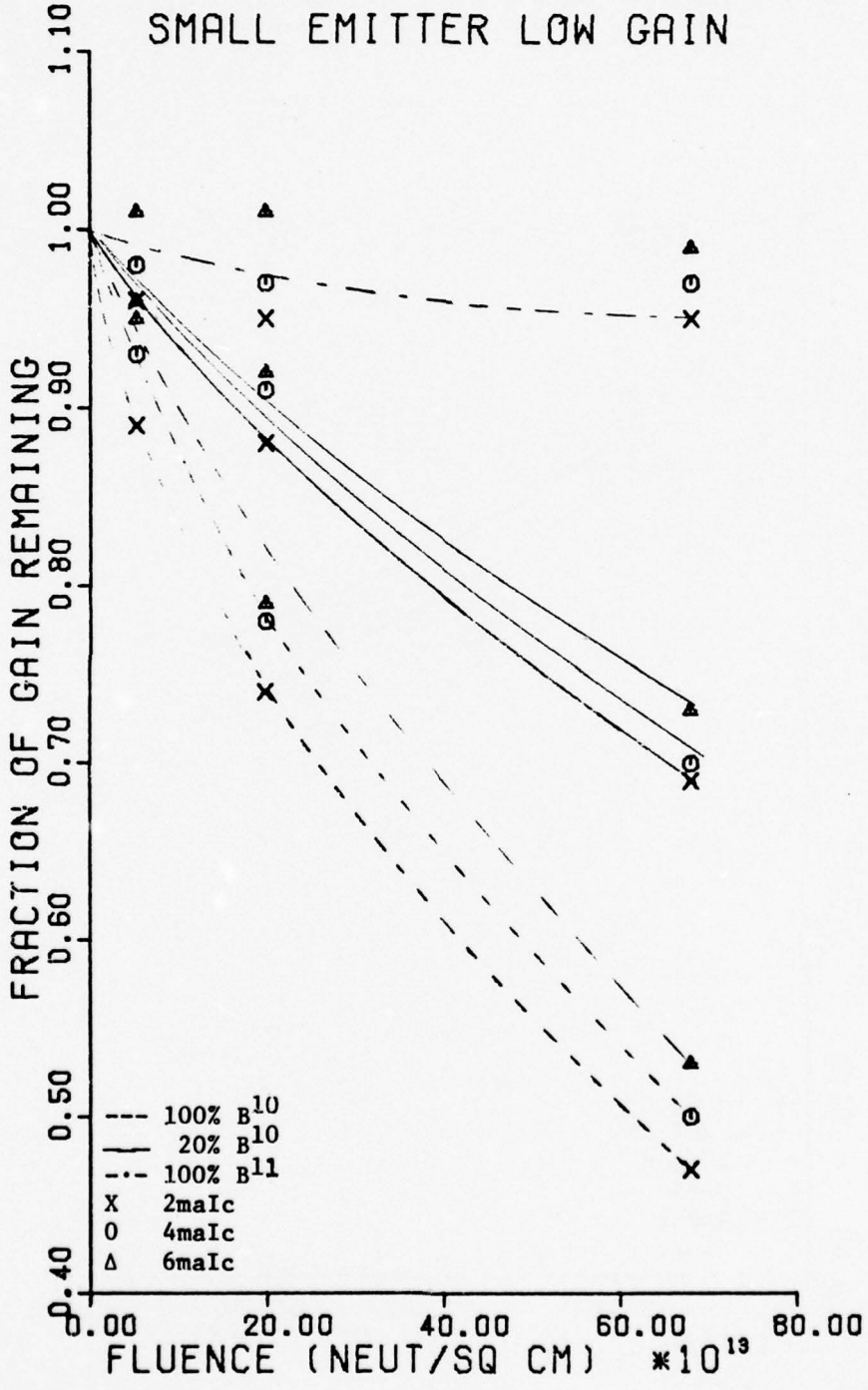


Figure 9. Gain Remaining vs. Fluence and Doping; Small-Emitter Low-Gain Transistors

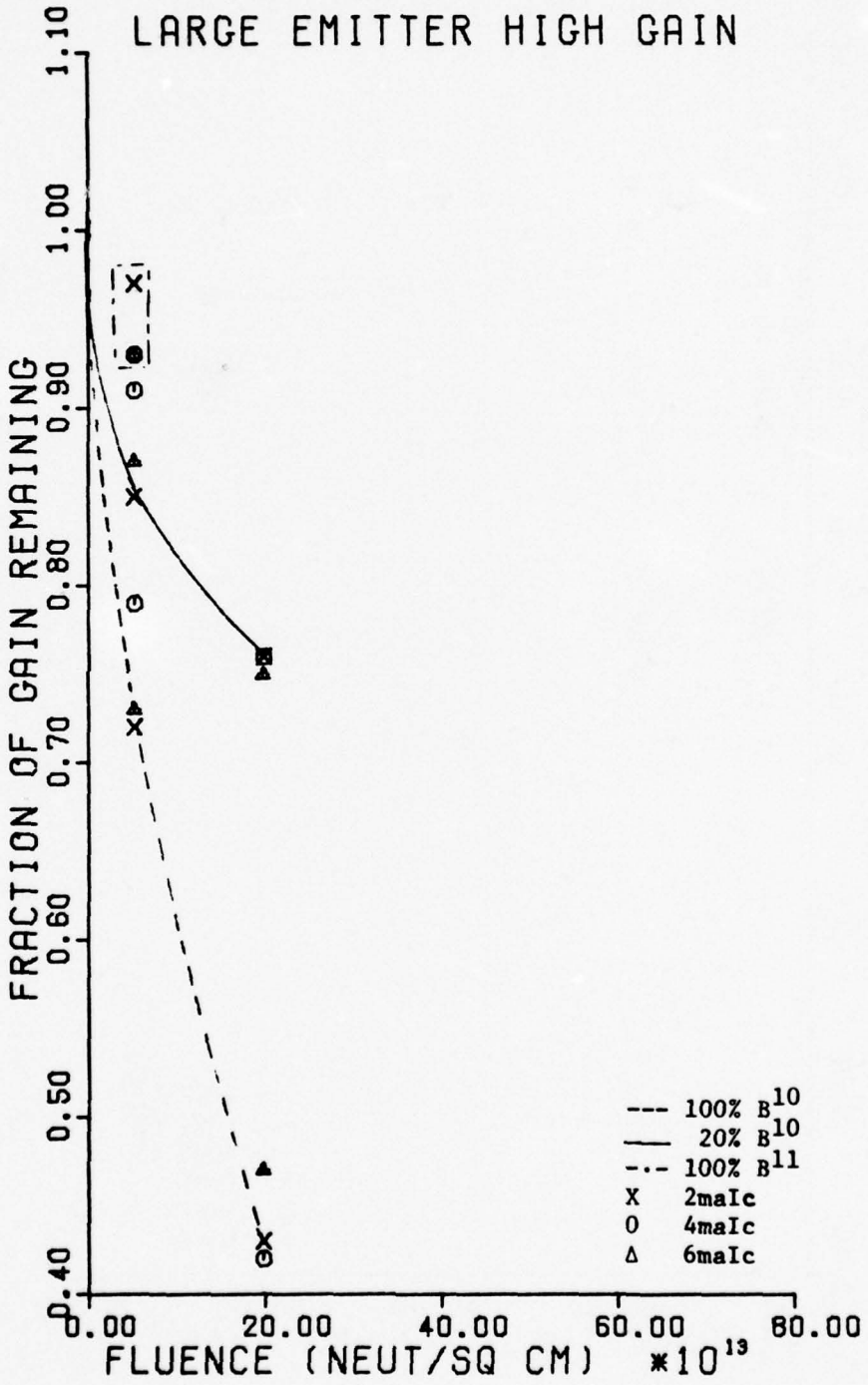


Figure 10. Gain Remaining vs. Fluence and Doping; Large-Emitter High-Gain Transistors

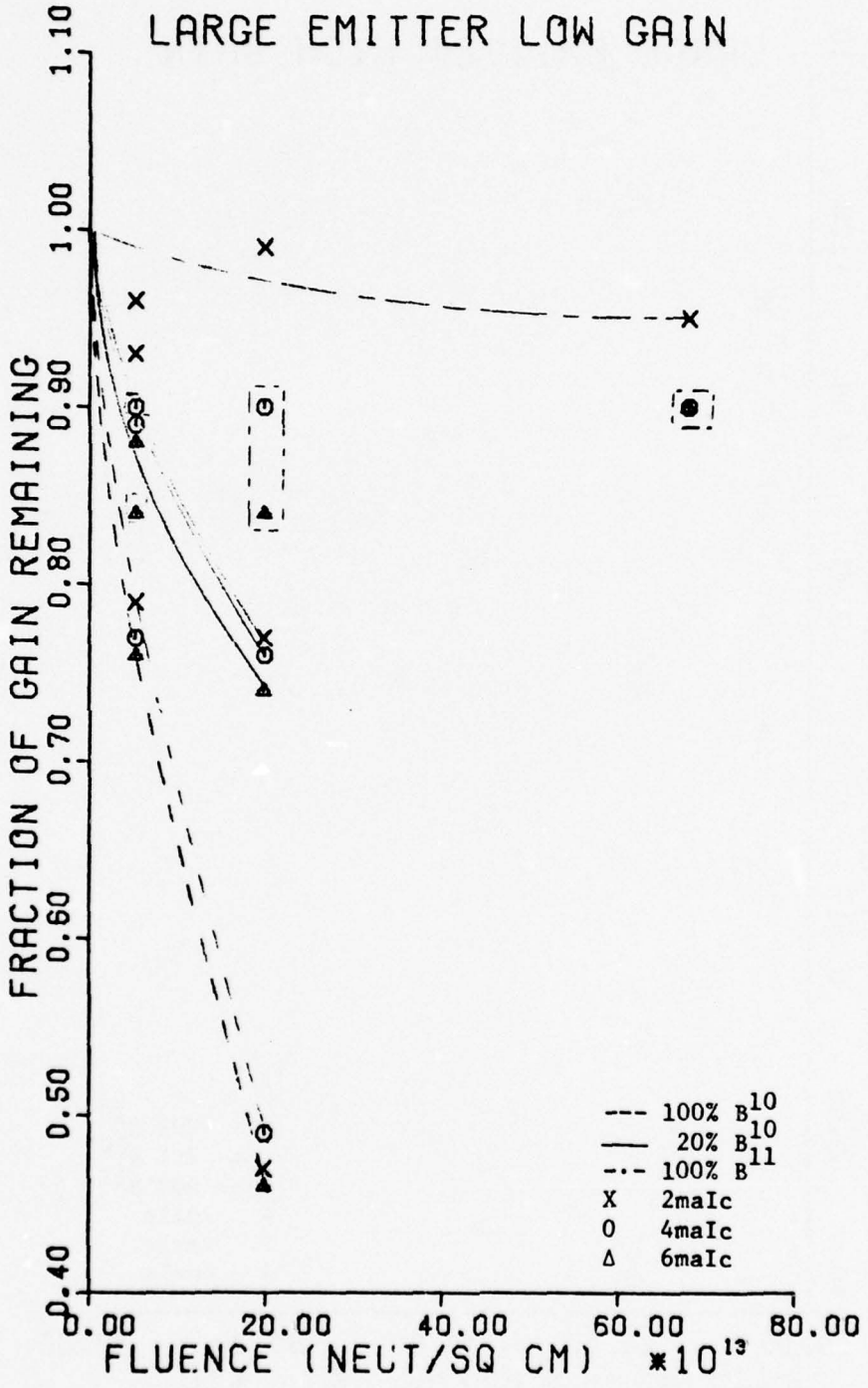


Figure 11. Gain Remaining vs. Fluence and Doping; Large-Emitter Low-Gain Transistors

large-emitter, high-gain, 100 percent Boron-11 transistor of this irradiation set failed due to an open circuit in the base (possibly due to mechanical shock in the rabbit tube). For this reason there was only one available data set plotted.

Figures 12, 13, 14, and 15 are graphs of $\Delta(1/\beta)$ as a function of thermal neutron fluence, also for the first set of irradiations. These graphs show that the damage, as measured by the reciprocal of the gain change [$\Delta(1/\beta)$] resulting from a given thermal neutron fluence, follows the bulk damage equation. In other words, the fact that $\Delta(1/\beta)$ is linearly proportional to the thermal neutron fluence, with the intercept at the origin, indicates that the source of the observed damage is bulk displacement damage. These graphs also show that the wider base transistors (i.e., those with low gain) are more susceptible to thermal neutron damage than the narrow-base (high-gain) transistors, as is expected. For those cases where the gain of the 100 percent Boron-11 transistors appeared to have slightly increased as a result of neutron irradiation, the $\Delta(1/\beta)$ was set equal to zero.

Since the proportionality constant between $\Delta(1/\beta)$ and neutron fluence is the radiation damage constant (C), the slopes of the curves are a measurement of C. The greater the damage, the smaller the percent error due to uncertainties in the measurements. Since the uncertainties in the relative values of the flux and in the gain measurements are on the order of 5 percent, those points near the horizontal axis are less reliable than those where the gain degradation is greater than 10 percent.

The second set of irradiations, which were performed by operations personnel of the National Bureau of Standards Reactor, were used to calculate the radiation damage constants for the various combinations of emitter dopant material and device geometry used. They were also compared with bulk damage constants for the fast neutron irradiations performed to obtain the relative effectiveness of fast and thermal neutrons in producing gain degradation in these devices. A summary of these results is given in table 1. Note the close agreement of the values of $C_{20\%B10}/C_{B10}$ to the expected value of 0.20.

Since the high- and low-gain devices have the same base dopant density and the same geometry, except for the differences in the width of the base regions, their relative values of initial gain and damage constants should be in the same ratio as the square of the base widths. This follows from the fact that

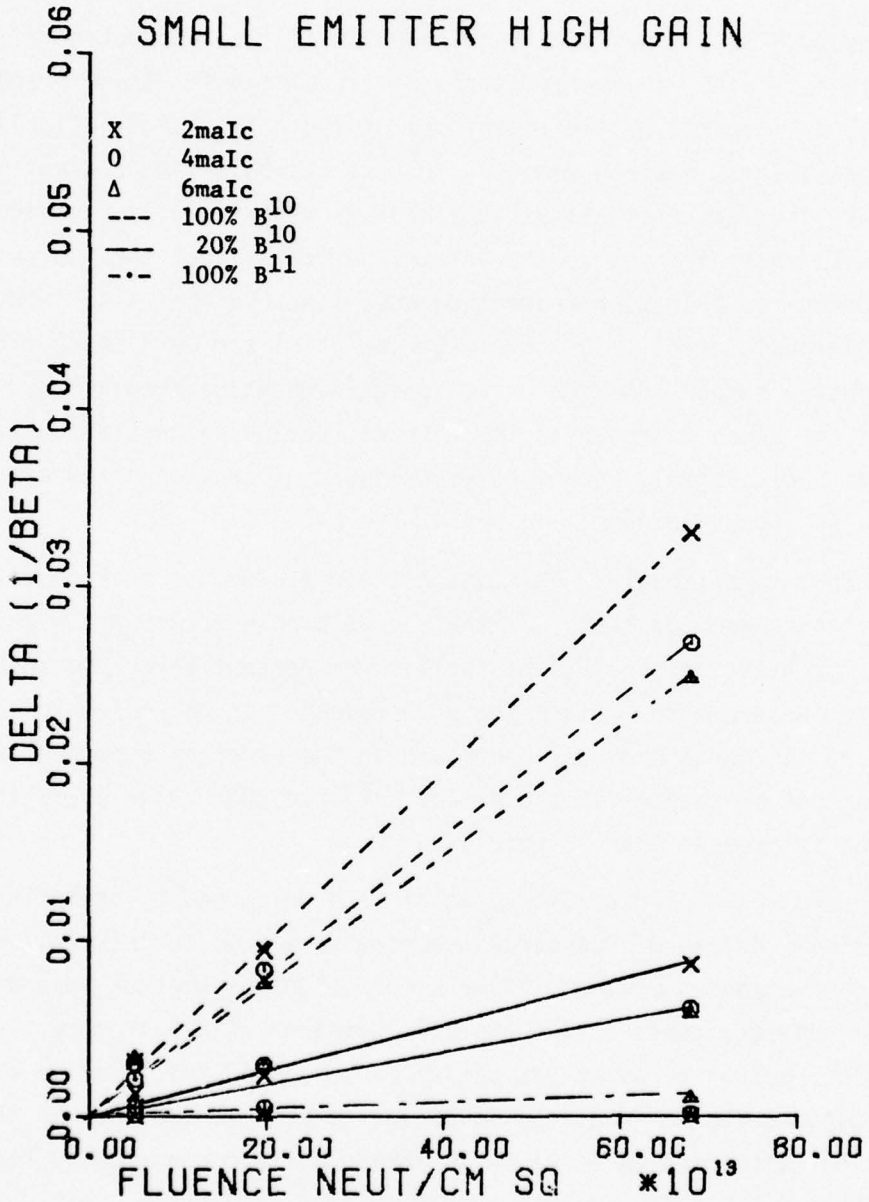


Figure 12. Δ(1/β) vs. Fluence and Doping for Small-Emitter High-Gain Transistors

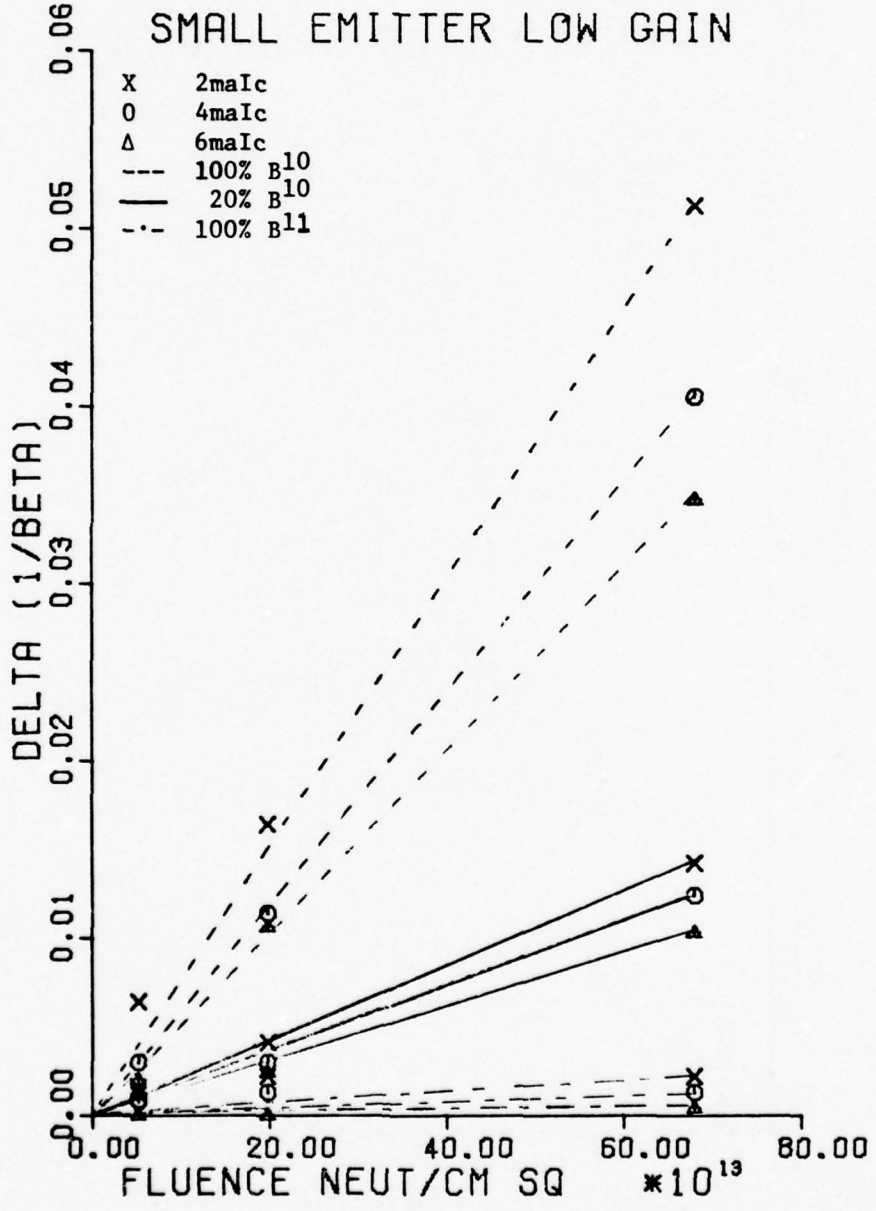


Figure 13. $\Delta(1/\beta)$ vs. Fluence and Doping for Small-Emitter Low-Gain Transistors

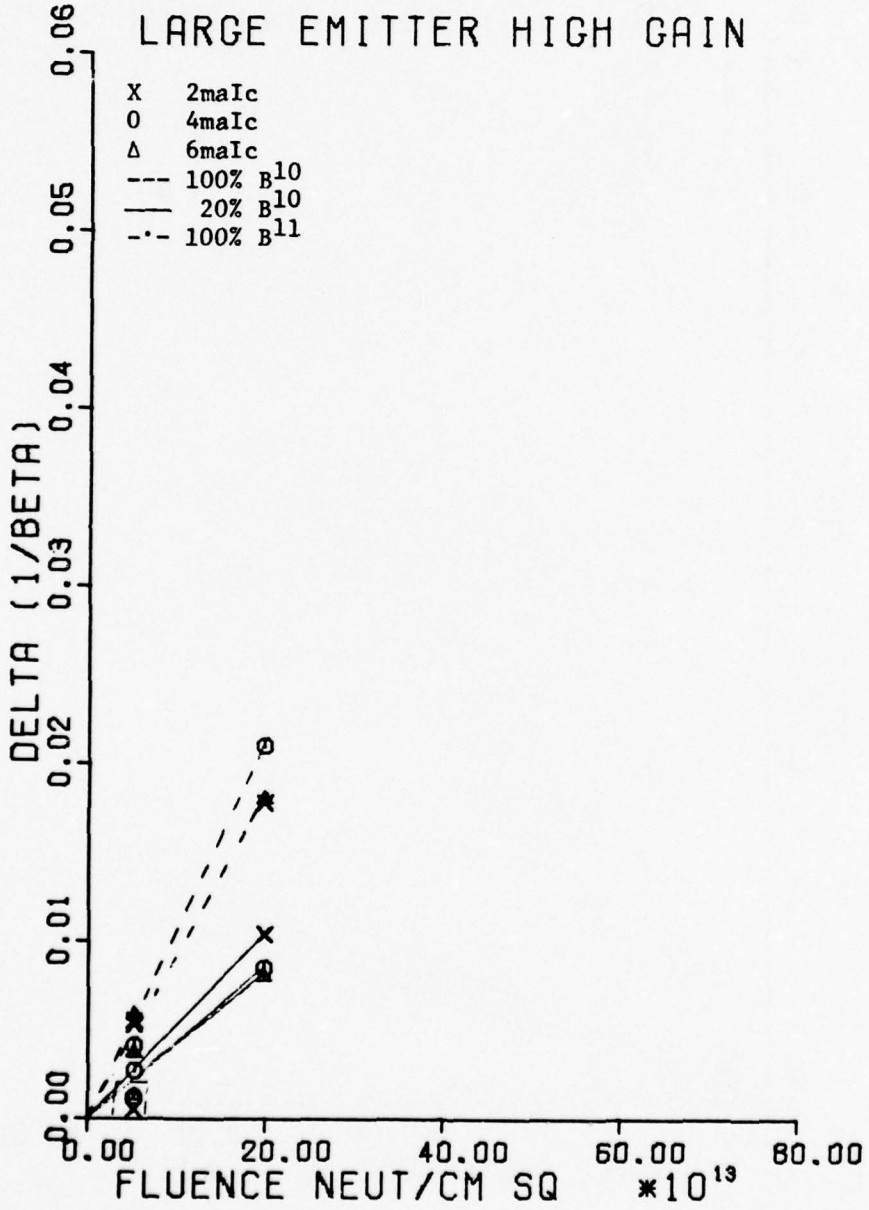


Figure 14. $\Delta(1/\beta)$ vs. Fluence and Doping for Large-Emitter High-Gain Transistors

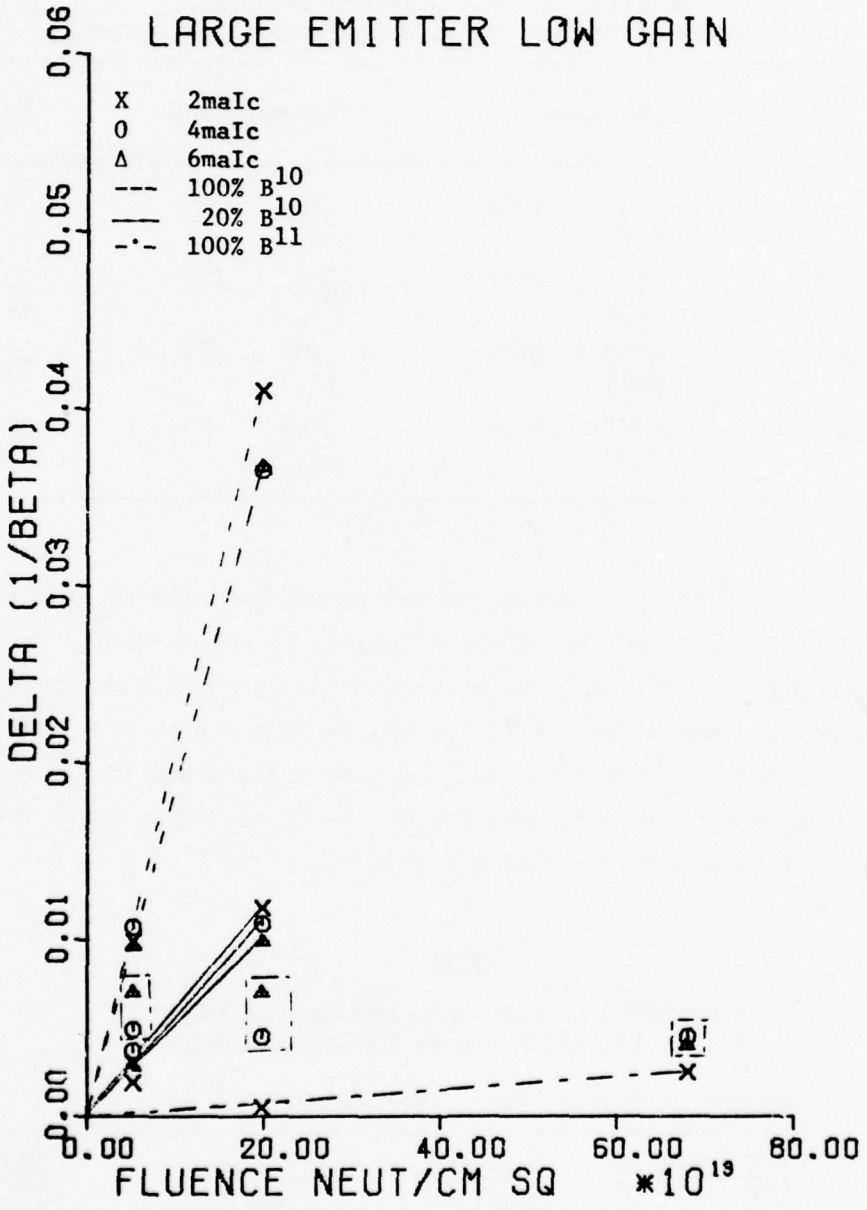


Figure 15. $\Delta(1/\beta)$ vs. Fluence and Doping for Large-Emitter Low-Gain Transistors

Table 1

RELATIVE VALUES OF THE DAMAGE CONSTANTS

Relative Value - Standard Deviation
(Number of Devices Used, Measurements per Device)

	C_{B11}/C_{B10}	$C_{20\%B10}/C_{B10}$	C_{fast}/C_{B10}
small emitter high gain	.0233 ± .0044 (5,5)	.190 ± .035 (12,4)	18.2 ± 1.42 (12,4)
small emitter low gain	.0306 ± .0017 (2,3)	.243 ± .003 (2,3)	22.6 ± 4.07 (4,1)
large emitter high gain	.0198 ± .0007 (2,3)	.197 ± .015 (2,3)	22.8 ± 3.88 (4,1)
large emitter low gain	.0142 ± .0025 (2,3)	.143 ± .004 (2,3)	22.9 ± 4.8 (4,1)

the time a minority carrier takes to travel across the base is proportional to the base width squared, and that the probability of recombination of a minority carrier is proportional to the time available for recombination. The ratio of the squares of the base widths is 1.65. The various ratios of initial gains and damage constants for the high- and low-gain transistors is summarized in table 2. The agreement is very good for the first two cases where there were many devices with many measurements per device.

Table 2

COMPARISON OF HIGH- AND LOW-GAIN DEVICES
BY INITIAL GAINS AND BY DAMAGE CONSTANTS

(Number of Devices Used, Measurements per Device)

	$\frac{\text{int. gain HG}}{\text{int. gain LG}}$	$\frac{C_{fast\ HG}}{C_{fast\ LG}}$	$\frac{C_{B10\ HG}}{C_{B10\ LG}}$	$\frac{C_{20\%B10\ HG}}{C_{20\%B10\ LG}}$
small emitter	1.65 ± .153 (18,11)	1.43 ± .26 (18,4)	1.80 ± .025 (6,3)	2.10 ± .011 (6,3)
large emitter	1.51 ± .182 (17,5)	1.59 ± .33 (17,3)	1.62 ± .10 (6,3)	2.27 ± .388 (6,3)

In figure 16 the current dependence of the various damage constants of the small-emitter high-gain transistor is shown. The damage constants were normalized to those of the 100 percent Boron-10 by multiplying each datum point by the quotient of the average Boron-10 damage constant and the average of the damage constants to be normalized. The normalization factors used are given in the figure. This figure demonstrates that the current dependence of the damage produced by the thermal neutrons is similar to that produced by fast neutrons. Insufficient comparable data points existed to make this comparison for the other transistor geometries.

The emitter and base resistances, as well as the emitter-base junction capacitances as a function of voltage and and breakdown voltage of the emitter-base junction, showed no significant change as a result of the irradiations. In all

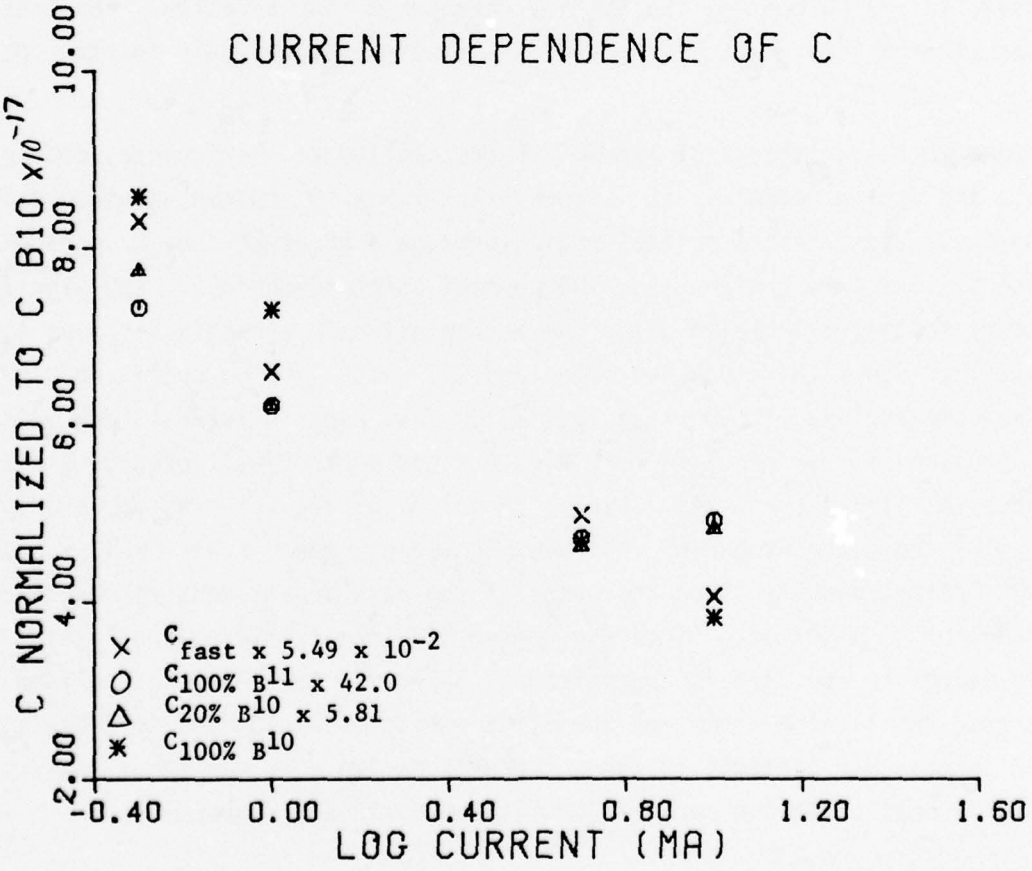


Figure 16. Current Dependence of Various Damage Constants for Small-Emitter High-Gain Transistors

but one of the 100 percent Boron-10, small-emitter, high-gain devices, the emitter-base junction leakage changed less than 50 percent. However, in the devices mentioned, the leakage went from 40 picoamperes to 4.2×10^6 picoamperes. As a result of this catastrophic leakage failure, the gain of this device went nearly to zero. In one of the 100 percent Boron-11 large-emitter devices, the collector and emitter contacts appeared to have become shorted together. Two additional devices appeared to have developed open circuits in one or more contacts. The source of these catastrophic failures is unknown.

The temperature monitors in the rabbit tubes indicated that the temperatures of the transistors stayed below 130° F during irradiation so that annealing effects should have been minimized. For the first set of irradiations, the postirradiation gains were measured within 6 hours of the irradiation; and for the second set, 1 week elapsed between the irradiation and the gain measurement. A recheck of one 100 percent Boron-10 device indicated that after 10 days had elapsed, 12 ± 3 percent of the initial damage had been annealed. For this reason, the devices in each irradiation set were compared only to other devices in the same set.

When the calculations of appendix C are applied to the fluence, doping level, and device geometry, it is found that 1.3×10^6 thermal neutron captures by Boron-10 atoms in the emitter region produce a 50 percent gain degradation in the small-emitter, high-gain, 100 percent Boron-10 devices. Applying the geometry factors calculated using the method given in appendix B, gives the result that 5.6×10^4 alpha particles and 1.1×10^5 lithium nuclei do damage in the base region. In contrast, 5.1×10^4 fast neutron interactions in the base produce similar results (ref. 9). A 1-MeV neutron will produce 5.0×10^3 defects in silicon (ref. 14). Since the volume of the base region is only 6.4×10^{-9} cm^3, the number of fast-neutron defects would be 4.0×10^{16} cm. As this defect density is on the order of the base dopant density observable degradation is expected. Since the number of alpha particles and lithium atoms doing damage in the base is approximately 3.3 times greater than the fast neutrons, the lithium atoms and the alpha particles would need to produce only 2,000 defects per particle to cause the same damage. As was shown in section II, 11,000 defects per alpha particle or lithium nucleus are possible.

---

14. Buehler, Martin G., Microelectronic Test Patterns: An Overview, NBS Special Publication 400-6, National Bureau of Standards, Washington, DC, August 1974.

The following equation for calculating the relative effectiveness of thermal neutrons to fast neutrons in producing defects in bipolar transistors can be obtained from these results.

$$\frac{C_{thermal}}{C_{1\ MeV}} = \frac{0.3\ (G_{\alpha} + G_{Li})\sigma_{thermal B10}\ N_{B10}\ W_{Emitter}}{\sigma_{1\ MeV\ si}\ N_{si}\ W_{Base}}$$

where G_{α} and G_{Li} are the geometry factors derived in appendix B, $\sigma_{thermal\ B10}$ is the Thermal Group capture cross section for Boron-10, $\sigma_{1\ MeV\ si}$ is the one MeV scatter cross section for silicon, N_{B10} is the atom density of Boron-10 atoms in the emitter, N_{si} is the atom density of silicon in the base, $W_{Emitter}$ is the width of the emitter, and W_{Base} is the width of the base. This formula, which is derived in appendix H, is good only for devices where the combined width of the emitter and base regions is less than the path length of a 0.88 MeV lithium nucleus in silicon (about 3.0 μm).

At the fluence at which the 100 percent Boron-11 devices begin to show damage (5×10^{15} neutrons per square centimeter), the density of thermal neutron captures by silicon atoms would be 2.3×10^{13} captures per square centimeter. Since a thermal neutron capture imparts an average of 780 eV of energy to a silicon atom, the defects produced by recoil of the lattice atoms resulting from these captures was possibly the main source of degradation of the all-Boron-11 devices. Also, thermal neutron captures by the Boron-10 in the collector dopant may have made a significant contribution to the observable damage. Bulk displacement from Compton scatter of gamma rays probably also contributed to the damage observed in the 100 percent Boron-11 transistors.

SECTION V

CONCLUSIONS AND RECOMMENDATIONS

For each of the 42 transistors exposed to thermal neutron irradiation, the damage observed was proportional to the fraction of the emitter dopant atoms that were Boron-10. It is therefore concluded that the hypothesized source of thermal neutron damage (ref. 1) in bipolar PNP transistors is the main source of the thermal neutron damage observed in this experiment. Also, the thermal neutron fluence and current dependence of the gain degradation indicated that bulk displacement damage was the source of damage. It was also observed that for these transistors, where the combined width of the emitter and base regions is less than the path length of a 0.88 MeV lithium nucleus in silicon, the dependence of gain degradation on the width of the base region was roughly the same for fast and thermal neutrons. One-MeV neutrons were found to be approximately 20 times more effective than thermal neutrons in degrading the gain of the transistors with 100 percent Boron-10 emitter dopant atoms and 100 times more effective in degrading the transistor doped with 20 percent Boron-10 and 80 percent Boron-11. By applying a geometry factor that was developed, it was found that a 1-MeV neutron produces about 3.3 times as many defects in silicon as are produced by the average particle (lithium or alpha doing damage in the base). An equation was developed to permit the calculation of the relative sensitivity of a given transistor to thermal neutron damage.

Since much of the material in the environment can conceivably thermalize neutrons from nuclear weapons, and since the effectiveness of thermal neutrons in producing damage can be reduced by using 100 percent Boron-11 as the dopant material, it would be desirable to use 100 percent Boron-11 doped transistors in underground or underwater electronic systems that must function in a nuclear environment. However, since pure Boron-11 would be expensive, it may be more cost effective to use the relative damage equation developed to obtain device geometries more resistant to thermal neutron damage.

APPENDIX A

A GENERAL PROOF OF THE β DEGRADATION EQUATION FOR BULK DISPLACEMENT DAMAGE

Copyright 1973 by the Institute of Electrical and Electronic Engineers, Inc.
Reprinted, with permission, from IEEE Transactions on Nuclear Science (ref. 15).

ABSTRACT

A general proof for the β degradation equation in displacement producing radiation environments is presented. The proof is straightforward for the base component of damage. An extension of the proof encompasses damage in the base emitter field region to the extent it can be related to the emitter time constant. The derivation assumes a significant post-radiation common emitter current gain (β > 3).

The relationship between common-emitter current gain and displacement damage has been given as[1]

$$\frac{1}{\beta} = \frac{1}{\beta_i} + \frac{\Phi}{\omega_T K} \tag{1}$$

where β is common-emitter current gain β_i is the initial unirradiated value of common-emitter current gain, ω_T is 2π times the common emitter gain bandwidth product, Φ is the damaging radiation fluence and K is the relevant lifetime damage constant. This relationship was initially proven for homogeneous base transistors and later extended to cover exponentially graded base transistors[2]. The following proof will show that this relationship is true for any base doping profile as long as the transistor retains a significant common-emitter current gain (β > 3).

Gover[3] has shown that for any arbitrary base impurity distribution, the series expansion for the base transport factor is

$$\alpha = 1 - U_1 \frac{W^2}{L^2} + U_2 \frac{W^4}{L^4} - \cdots\cdots \tag{2}$$

where α is the base transport factor, W is the base width and $L = \sqrt{D\tau}$ is the diffusion length. The coefficients U_1, U_2 etc., are determined by successive iteration of the equation pair.

$$n(X) = -\frac{1}{qN}\int_X^{X_2} \frac{N}{D}\, J\,dX \tag{3}$$

$$J(X) = J^0 + q\int_{X_1}^{X_2} \frac{n}{\tau}\,dX$$

where n is the excess minority carrier concentration in the base, N is the impurity density in the base, D is diffusion constant, τ is minority carrier lifetime, q is electron charge, and J is minority current density.

Specifically, this procedure leads to the following deterministic equations for U_1 and U_2:

$$U_1 = \frac{D(X_2)\tau(X_2)}{W^2}\int_{X_1}^{X_2} \frac{dX}{\tau(X)\,N(X)} \int_X^{X_2} \frac{N(\bar{X})\,d\bar{X}}{D(\bar{X})} \tag{4}$$

$$U_2 = \frac{D^2(X_2)\tau^2(X_2)}{W^4}\int_{X_1}^{X_2} \frac{dX}{\tau(X)\,N(X)} \int_X^{X_2} \frac{N(\bar{X})\,d\bar{X}}{D(\bar{X})}$$

$$\int_{X_1}^{\bar{X}} \frac{d\bar{\bar{X}}}{\tau(\bar{\bar{X}})\,N(\bar{\bar{X}})} \int_{\bar{\bar{X}}}^{X_2} \frac{N(\bar{\bar{X}})\,d\bar{\bar{X}}}{D(\bar{\bar{X}})}$$

A recombination series corresponding to Equation (2) exists for n and j.

$$J(X) = J^0(X) + J^1(X) \cdots\cdots$$

$$n(X) = n^0(X) + n^1(X) \cdots\cdots \tag{5}$$

Now,

$$1 - \alpha = \frac{-(J^1 + J^2 + J^3 \cdots)}{J^0} = -\frac{J^1}{J^0} \tag{6}$$

The series expansion is rapidly convergent and can be terminated at J^1 since

$U_2 \frac{W^4}{L^4} \ll U_1 \frac{W^2}{L^2}$ except for transistors so seriously damaged that they are no longer of practical interest.

From Equation (2) and assuming that base transport is the dominant factor in the radiation dependence of common emitter current gain

$$\frac{1}{\beta} = \frac{U_1 W^2}{D\tau} \tag{7}$$

Gover[3] also shows that when n/τ is described by a single time constant, i.e.,

$$\frac{1}{q}\frac{\partial J}{\partial X} = \frac{n}{\tau}(1 + j\omega\tau),\quad \omega_T = \frac{D}{U_1 W^2} \tag{8}$$

again truncating the recombination series at the first-order term.

Now minority carrier lifetime as a function of displacement fluence is given by

$$\frac{1}{\tau} = \frac{1}{\tau_i} + \frac{\Phi}{K} \tag{9}$$

---

15. Messenger, George C., "A General Proof of the Degradation Equation for Bulk Displacement Damage," IEEE Transactions on Nuclear Science, NS-20 1, February 1973.

for all damaging radiations including neutrons protons, electrons and γ rays with the appropriate choice of K.

Combining this result with Equation (7) gives

$$\frac{1}{\beta} = \frac{1}{\beta_1} + \frac{U1\,W^2}{D}\,\frac{\Phi}{K} \qquad (10)$$

Note that $\frac{1}{\beta_1}$ may also contain a surface recombination, and an emitter efficiency contribution as long as they do not change significantly with displacement fluence.

Combining this result with Equation (8) gives

$$\frac{1}{\beta} = \frac{1}{\beta_1} + \frac{\Phi}{\omega_T K} \qquad \text{Q. E. D.} \qquad (11)$$

The base impurity distribution is arbitrary, both τ and D may be functions of X, but the transistor must have significant common-emitter current gain, i.e.,

$$U_2\frac{W^4}{L^4} << U_1\frac{W^2}{L^2}$$

Values of U_1 and U_2 are given in Table 1 for homogeneous and exponential impurity distributions. The error function impurity distribution produces U_1 and U_2 values very similar to the exponential distribution.

	Homogeneous Base	Exponential Base
	N = Const.	$N = N_0\, e^{-\eta x/W}$
U_1	$\frac{1}{2}$	$\frac{\eta + e^{-\eta} - 1}{\eta^2}$
U_2	$\frac{5}{24}$	$\frac{\frac{1}{2}\eta^2 - 2 + (3\eta + 1)e^{-\eta} + e^{-2\eta}}{\eta^4}$

Table 1

Values of U_1 and U_2 for Homogeneous and Exponential Impurity Distribution with D and τ constant.

Ramsey and Vail[4] have shown that the emitter efficiency contribution resulting from recombination in the emitter base field region can be related to the emitter time constant, r_eC_e. Equation (8) strictly relates to the cut-off frequency for base transport; it can be readily extended to include the emitter time constant.

$$\omega_T^{-1} = \left(r_eC_e + \frac{U_1W^2}{D}\right)^{-1} \qquad (12)$$

Including both emitter-base field recombination and base recombination and extending Equation (7) including the Ramsey and Vail[4] relationships.

$$\frac{1}{\beta} = \frac{U_1W^2}{D\tau} + \frac{I_p}{I_n} = \frac{1}{\tau}\left(r_eC_e + \frac{U_1W^2}{D}\right) \qquad (13)$$

Combining Equations (12), (13) and (9) yields

$$\frac{1}{\beta} = \frac{1}{\beta_1} + \frac{\Phi}{\omega_T K} \qquad \text{Q. E. D.} \qquad (14)$$

This extends the proof to cover both emitter-base field recombination and bulk recombination subject to the additional approximations used by Ramsey and Vail[4] to obtain Equation (13).

References

(1) Messenger, G. C. and Spratt, J. P. "The Effects of Neutron Irradiation on Germanium and Silicon," New York Meeting of Electrocnemical Society, April 1958. Published in Proceedings IRE, June 1958, pp 1038-1044.

(2) Messenger, G. C. "Current Gain Degradation due to Displacement Damage for Graded Base Transistors," Proc. IEEE Vol. 55 No. 3, March 1967, pp 160.

(3) Gover, et al "Bipolar Transistor Base Parameters and Impurities," PGED-19 Vol. 8, August 1972, pp 967-975.

(4) C. Ramsey and P. Vail "Current Dependence of the Neutron Damage Factor," PGNS Vol. NS-17 No. 6, pp 310-135.

APPENDIX B

GEOMETRY FACTOR CALCULATION

The geometry factor is the portion of particles produced in the emitter that do all of their damage in the base region. This calculation of the geometry factor requires the following assumptions:

1. All directions of particle emission are equally probable.
2. The path length of the particles is short compared to the surface area of the devices.
3. The range of the particle is greater than the thickness of the emitter and base regions.
4. The particle does all of its displacement damage at the end of its path length.

Then the locus of points at which a particle originating at a given location can do damage would form a sphere of radius equal to the range of the particle, with its center at the point of origin. By assumption 3, the sphere must contain a complete thickness of the slab of the base region (figure 17).

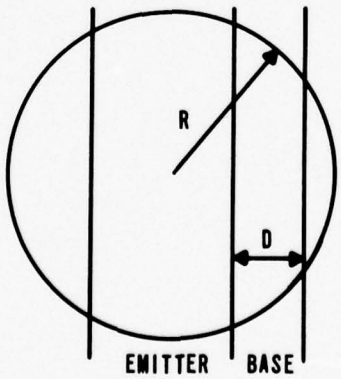


Figure 17. Geometry Factor Relationships

Let the range of the particle be R and the thickness of the base region be D. Then the area S of the intersection of the sphere with the base region is just

$$S = 2 \pi R D$$

This is true, regardless of the position of the slab in the sphere, as long as a complete base region width is contained in the sphere as required by assumption 3. The total area of the sphere A is

$$A = 4 \pi R^2$$

Since A is a measure of all possible damage sites and S is a measure of those in the base region, the fraction produced that ends in the base region is just S/A or

$$G = \frac{D}{2R}$$

where G is the fraction of total particles produced that do damage in the base region. Note that the distribution of sources across the emitter region is unimportant as long as assumptions 1 through 4 are met.

APPENDIX C

THERMAL NEUTRON REACTION RATE IN PNP TRANSISTORS

The B^{10} (n,α) Li^7 reaction is exothermic with an energy release of 2.78 MeV. In reactions involving thermal neutrons, the probability of forming Li^7 in the ground state is only 0.064. Instead, an intermediate excited state of Li^7 is formed, followed by the emission of a 0.48 MeV gamma ray. Thus, the total kinetic energy available to the Li^7 nucleus and the alpha is as follows

$$E_{Li} = \frac{E_{KE} M_{\alpha}}{M_{\alpha} + M_{Li}} = \frac{(2.30)(4.00)}{(4.00) + (7.02)} = 0.83 \text{ MeV} \tag{1}$$

$$E_{\alpha} = \frac{E_{KE} M_{Li}}{M_{Li} + M_{\alpha}} = 1.47 \text{ MeV} \tag{2}$$

Up to 30 keV, the cross section (σ) for this reaction has a 1/v dependence, where v is the thermal neutron velocity. This can be represented as follows

$$\sigma = \frac{\sigma_0 v_0}{v} \tag{3}$$

where $v_0 = 2.2 \times 10^5$ cm/sec and $\sigma_0 = 3840$ barns $= 3.84 \times 10^{-21}$ cm^2.

This 1/v dependence can be used to calculate the reaction rate, dR, resulting from neutrons with energies between E and E + dE in the volume element dV

$$dR = N(x,y,z)\ \sigma(E)\ \phi(E,x,y,z)\ dE\ dV \tag{4}$$

where $N(x,y,z)$ = the number of B^{10} atoms per unit volume at the point (x,y,z); $\sigma(E)$ = the B^{10} (n,α) cross section at energy E corresponding to the velocity V through the equation $E = \frac{1}{2} m_n \sigma^2$; and $\phi(E,x,y,z)$ = the flux per unit energy interval at the point (x,y,z). Since the flux is, for these purposes, assumed to be independent of position, write

$$\phi(E,x,y,z) = \phi(E) \tag{5}$$

Write

$$\phi(E) = n(E)v \tag{6}$$

where n(E) is the number of thermal neutrons per unit volume per unit energy interval with energies between E and E + dE. Combining equations 3 and 6,

$$\phi(E)\ \sigma(E) = [n(E)v]\left[\sigma_0 v_0/v\right] = n(E)\ \sigma_0 v_0 \tag{7}$$

The resulting expression for dR is thus

$$dR = N(x,y,z)\ n(E)\ \sigma_0 v_0\ dE\ dV \tag{8}$$

This may be integrated to yield the total number of reactions, R, produced by an arbitrary spectrum of neutrons with energies below 30 keV

$$R = \sigma_0 v_0 \int_{Vol}\int_0^{30\ keV} N(x,y,z)\ n(E)\ dE\ dV = \sigma_0 v_0 \quad {}_{Vol}N(x,y,z)\ dV \quad {}_0^{30\ keV}n(E)\ dE \tag{9}$$

Here

$${}_{Vol}N(x,y,z)\ dV = N_B \tag{10}$$

where N_B = total number of Boron-10 atoms in sample, and

$$\int_0^{30\ keV} n(E)\ dE = n \tag{11}$$

where n is the number of neutrons per unit volume, irrespective of energy up to 30 keV incident on the sample.

Thus

$$R = N_B\ \sigma_0 v_0\ n \tag{12}$$

Note that equation 12 is independent of both the neutron spectrum and of the distribution of the boron atoms in the sample. Equation 12 can be expressed in terms of the neutron flux, $\phi = n\ \bar{v}$, where $\bar{v}$ is the average neutron velocity

$$R = \frac{N_B \sigma_0 v_0 \phi}{\bar{v}} \tag{13}$$

For a Maxwell-Boltzman distribution in thermal neutron energy, $\bar{v}$ is 1.128 v_0 at 20° C. For this spectrum

$$R = \frac{N_B \sigma_0 \phi}{1.128} \tag{14}$$

This equation can also be expressed in terms of the total neutron fluence, Φ, incident on the sample in time t. Here assume that the neutrons are deposited uniformly in time and write

$$\Phi = \phi t \tag{15}$$

Thus, write

$$R = \frac{N_B \sigma_0 \Phi}{(1.128)t} \tag{16}$$

The total number, N, of alphas produced is

$$N_\alpha = Rt = \frac{N_B \sigma_0 \Phi}{(1.128)} \tag{17}$$

or since $\sigma_0 = 3.84 \times 10^{-21}$ cm^2 (ref. 16)

$$N_\alpha = (3.4 \times 10^{-21} \text{ cm}^2)\, N_B\, \Phi \tag{18}$$

Note that only 18.45 to 18.98 percent of naturally occurring boron is B^{10}. The bulk of naturally occurring boron is B^{11}.

Now consider a specific example of a PNP bipolar transistor whose emitter is heavily doped with boron. Typical dopant concentrations at the junction between the emitter and the base are 10^{20} boron atoms per cm^3. Also assume that this transistor is irradiated by thermal neutrons with a Maxwell-Boltzman

16. Hughes, Donald J. and Robert B. Schwart, Neutron Cross Sections, BNL 325, Brookhaven National Laboratory Associated Universities, Upton, Long Island, New York, 1 July 1958.

spectrum to a fluence of 5×10^{11} n/cm^2. Further, assume that the PNP transistor is of planar construction, with a base width of 0.7 microns and an emitter width of 1.3 microns. Since the range of an alpha particle from the B^{10} (n,α) Li^7 reaction is 10 microns, the alpha penetrates far into the collector where most of its energy is dissipated. Assume also that the emitter is 1 mil by 1.5 mils in area. Since there are 25.4 microns to a mil, these dimensions are large compared to the range of the alpha. Thus, calculate by use of equation 18 the total number of boron (n,α) reactions which occur.

$$\begin{aligned} N_\alpha &= (3.4 \times 10^{-21}\ \text{cm}^2)\ \Phi\ N_B \\ &= (1.7 \times 10^{-9})\ N_B \\ &= (1.7 \times 10^{-9}) \left(10^{20}\ \frac{B}{\text{cm}^3}\right) (2.5 \times 10^{-3}\ \text{cm}) \times \\ &\quad (3.75 \times 10^{-3}\ \text{cm})\ (1.3 \times 10^{-4}\ \text{cm})\ (.1898\ B^{10}/B) \end{aligned} \tag{19}$$

$$N_\alpha = 39.3\ \text{alphas} = N_{Li} = 39.3\ Li^7\ \text{atoms}$$

Since half of these alphas are directed toward the surface, the result is that there are only 20 which penetrate the base region. Since this is such a small number of alphas, any damage or ionization produced may be neglected. For example, assume for a worst case ionization condition that all of the energy of the alpha and the lithium recoil atom goes into ionization. The result will be no more than a thousand rads silicon deposited in the transistor even when the short range of the lithium recoil is considered in a calculation of effective collection volume. Note that a rad is an expression of energy per gram, and as the collection volume decreases, the rads deposited will increase in this case. Increasing the emitter area does not have any effect on the rads deposited for this same reason. It is also easy to see that the damage due to 20 alphas and 20 Li^7 nuclei will also be negligible. Increasing the area also has no effect on the ratio of damage to area, which determines the degradation. Only an increase of doping level and emitter thickness to unrealistic dimensions will yield enough alphas to degrade the transistor.

APPENDIX D

NBS-2 TEST PATTERN

Note: All dimensions in mils. Center of mask is taken as (0,0); horizontal coordinate is given first followed by vertical coordinate. One square equals 1 mil. Lines not on grid lines are halfway between grid lines. C = Center. R = Radius. S = Distance from C to one side of square.

Table 3

TEST STRUCTURES

(Numbers Refer to Figure 18)

Number	Test Structure	Dimension,* mil
1	Gated circular base-collector junction with diffused channel stop	D = 6
2	Ungated circular base-collector junction with diffused channel stop	D = 6
3	Ungated square base-collector junction with diffused channel stop	S′ = 5
4	Gated square base-collector junction with diffused channel stop	S′ = 18
5	Ungated circular base-collector junction with diffused channel stop	D = 20
6	Gated circular base-collector junction with diffused channel stop	D = 20
7	Gated circular base-collector junction (small emitter) with diffused channel stop	D = 20
8	Gated circular base-collector junction (large emitter) with diffused channel stop	D = 20
9	Gated circular base-collector junction with diffused channel stop	D = 60
10	MOS capacitor over collector with field plate and diffused channel stop	D = 6
11	MOS capacitor over collector with field plate and diffused channel stop	D = 20
12	MOS capacitor over collector with distant field plate and diffused channel stop	D = 20
13	MOS capacitor over base without field plate and diffused channel stop	D = 20
14	Base sheet resistor	
15	Emitter sheet resistor	
16	Metal-to-base contact resistor	
17	Metal-to-emitter contact resistor	
18	Collector resistor	
19	Base-under-the-emitter sheet resistor (tetrode transistor)	
20	Hall effect pattern	
21	Alignment marker	

*D = diameter of a circle, S′ = side of a square. Tolerances should be held to ± 0.1 mil. If metric dimensions are desired, the diameters should be 0.15 mm (for structures numbered 1, 2, 10), 0.5 mm (5-8, 11-13), and 1.5 mm (9); and the sides should be 0.13 mm (3) and 0.46 mm (4); all tolerances should be held to ± 0.002 mm.

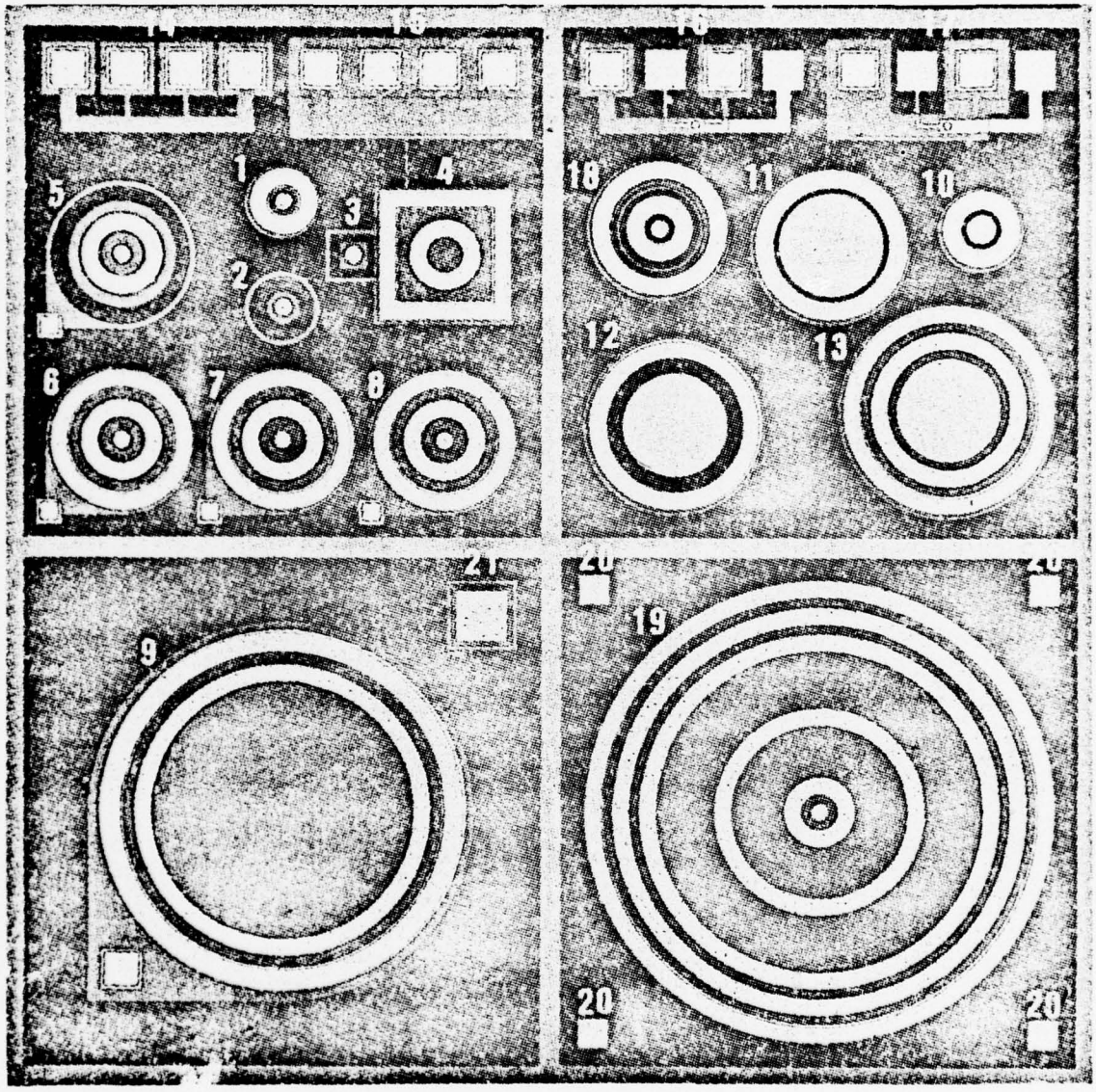


Figure 18. Test Pattern, NBS-2, for Characterizing the Electrical Properties of Silicon MOS Capacitors and p-n Junctions. (The 21 elements are identified in table 3. The overall pattern is 200 mil [5.08 mm] on a side.)

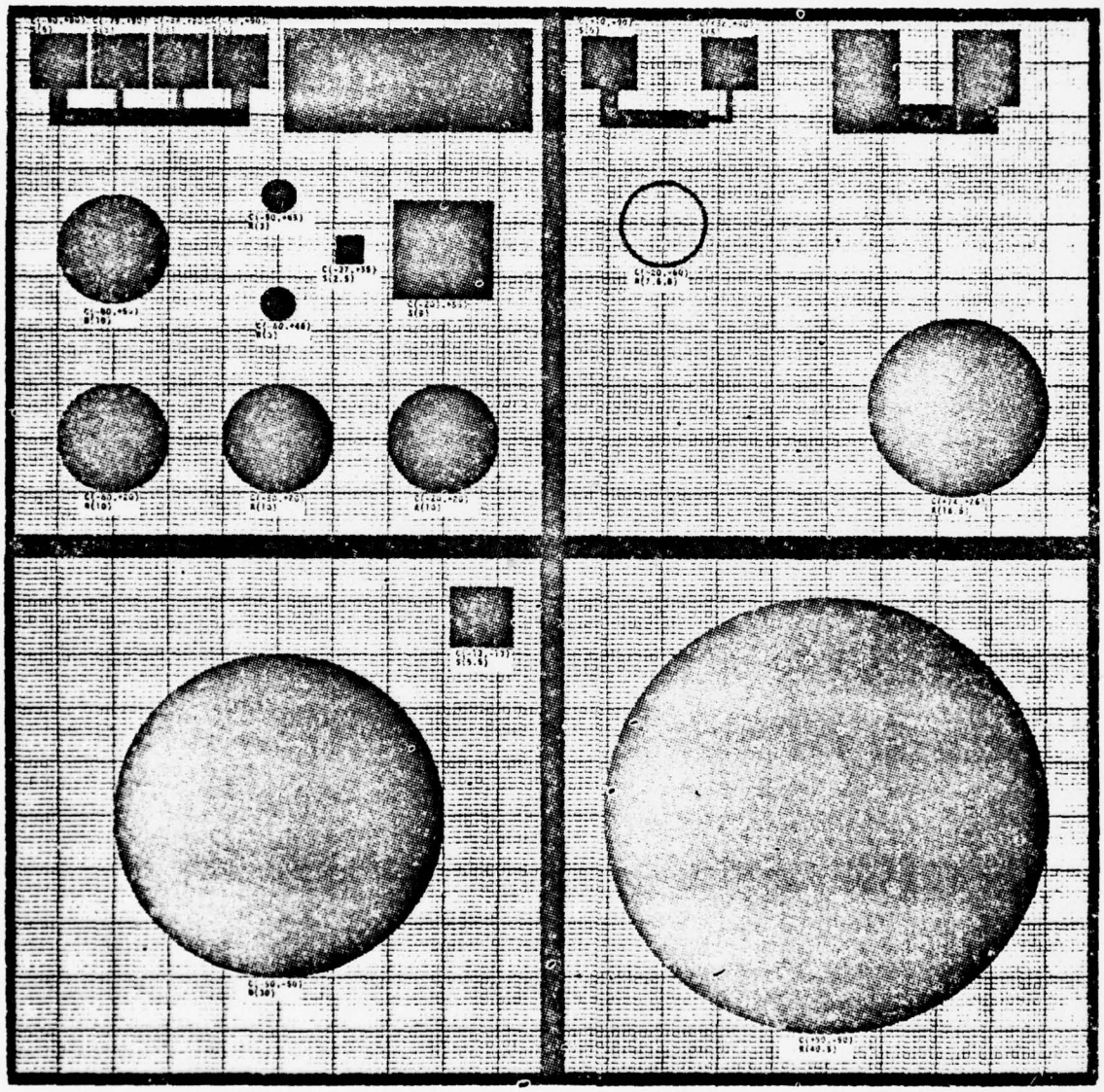


Figure 19. Base Mask

(For positive photoresist, black areas are clear on final mask.)

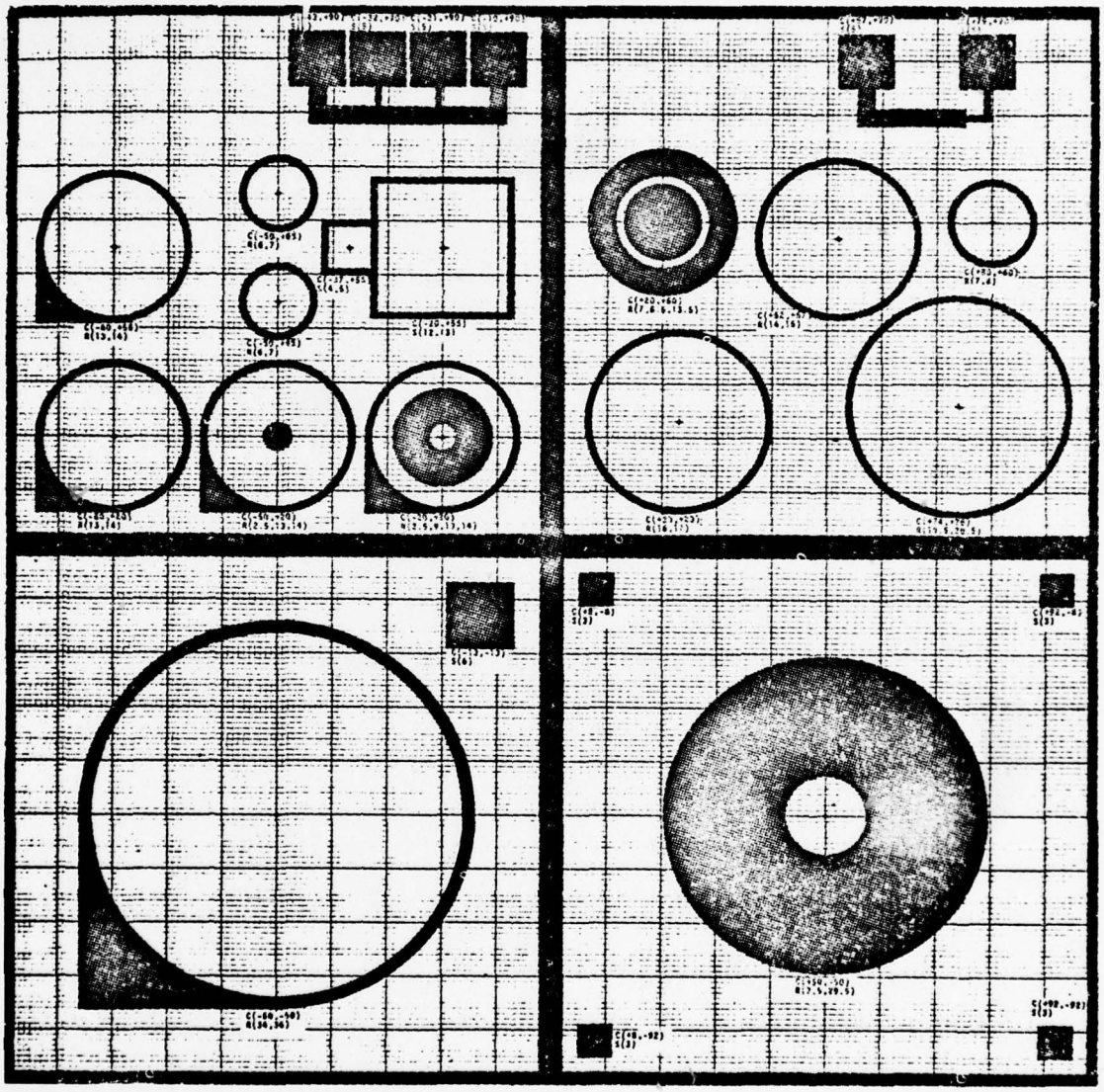


Figure 20. Emitter Mask

(For positive photoresist, black areas are clear on final mask.)

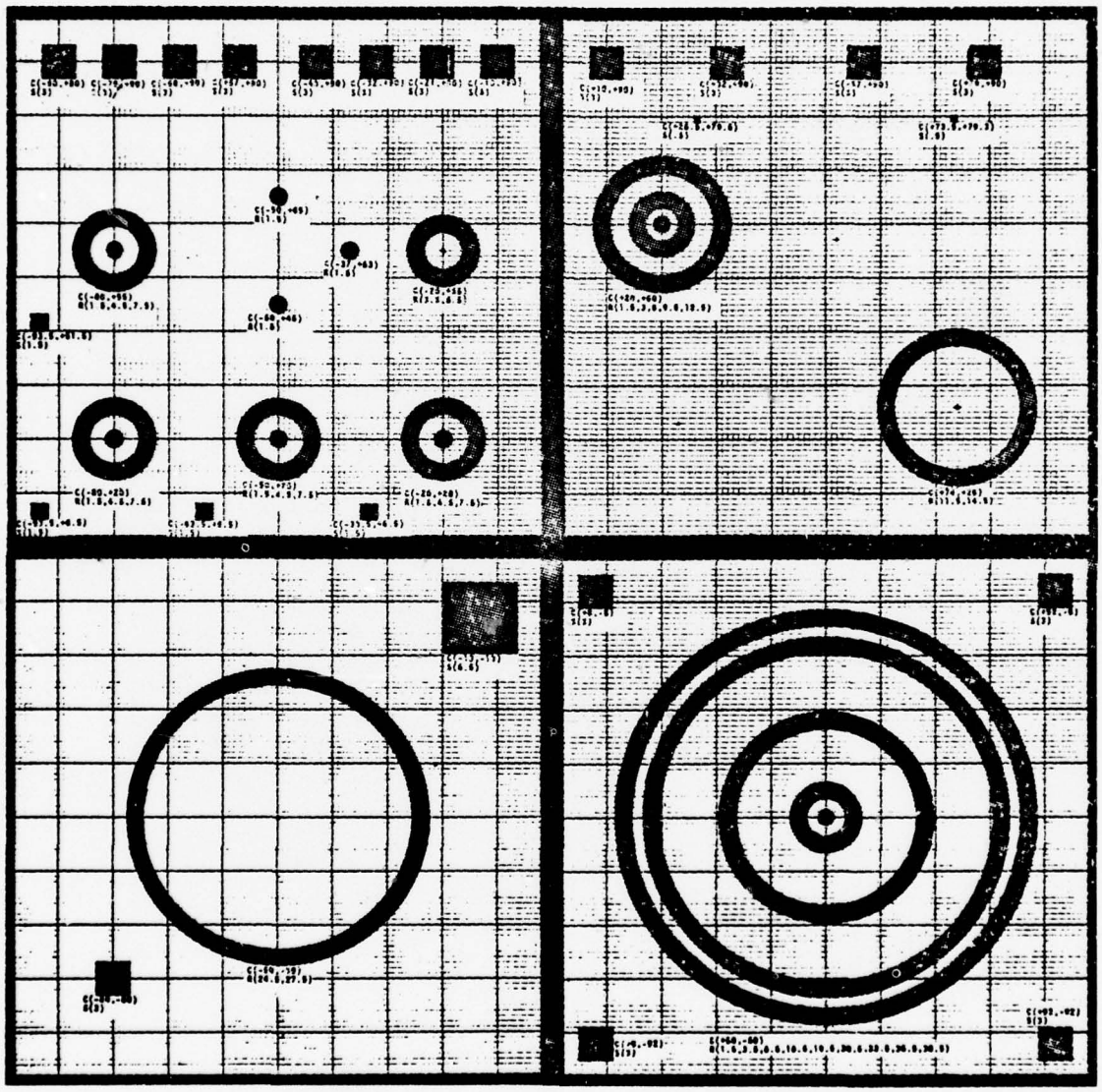


Figure 21. Contact Mask

(For positive photoresist, black areas are clear on final mask.)

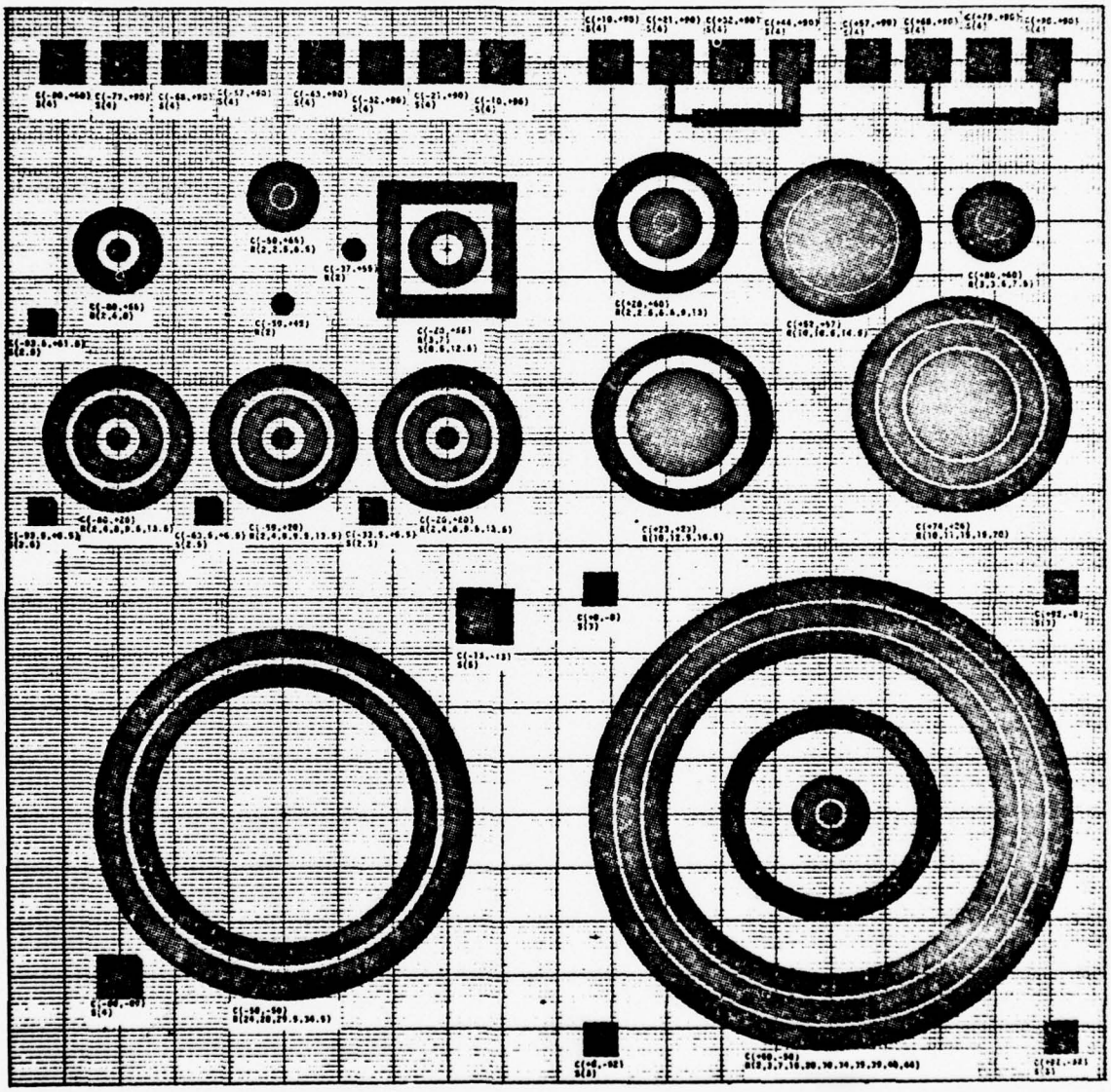


Figure 22. Metal Mask

(For positive photoresist, black areas are black on final mask.)

APPENDIX E

TRANSISTOR PROCESS INFORMATION

CONTROL WAFER MEASUREMENTS

C1 - Base Implant, drive-in A
Rs = 193 Ω/□
Xj = 1.55 μm

Drive-in B: we,4,2,8,4,12
Drive-in A: w1,2,5,6,9,10

C2 - ^{11}B Emitter + base, drive-in A
Rs = 24.8 Ω/□
Xj = 1.05 μm

C3 - ^{11}B Emitter + base, drive-in B
Rs = 24.6 Ω/□
Xj = 1.09 μm

C4 - ^{10}B Emitter + base, drive-in A
Rs = 25.0 Ω/□
Xj = 0.90 μm

C5 - 80% ^{11}B + 20% ^{10}B emitter + base, drive-in A
Rs = 25.3 Ω/□
Xj = 0.93 μm

For Base: $\bar{\sigma} = \frac{1}{RsXj} = 33.4\ (\Omega\text{-cm})^{-1}$

from Irvin's Curves (Gaussian) $Cs \approx 2 \times 10^{18}\ cm^{-3}$ (for 10^{12} substrate)

For Emitter: $\bar{\sigma} = \frac{1}{RsXj} \simeq 400\ (\Omega\text{-cm})^{-1}$

from Irvin's Curves (Gaussian) $Cs \approx 10^{20}\ cm^{-3}$ (for 10^{12} substrate)

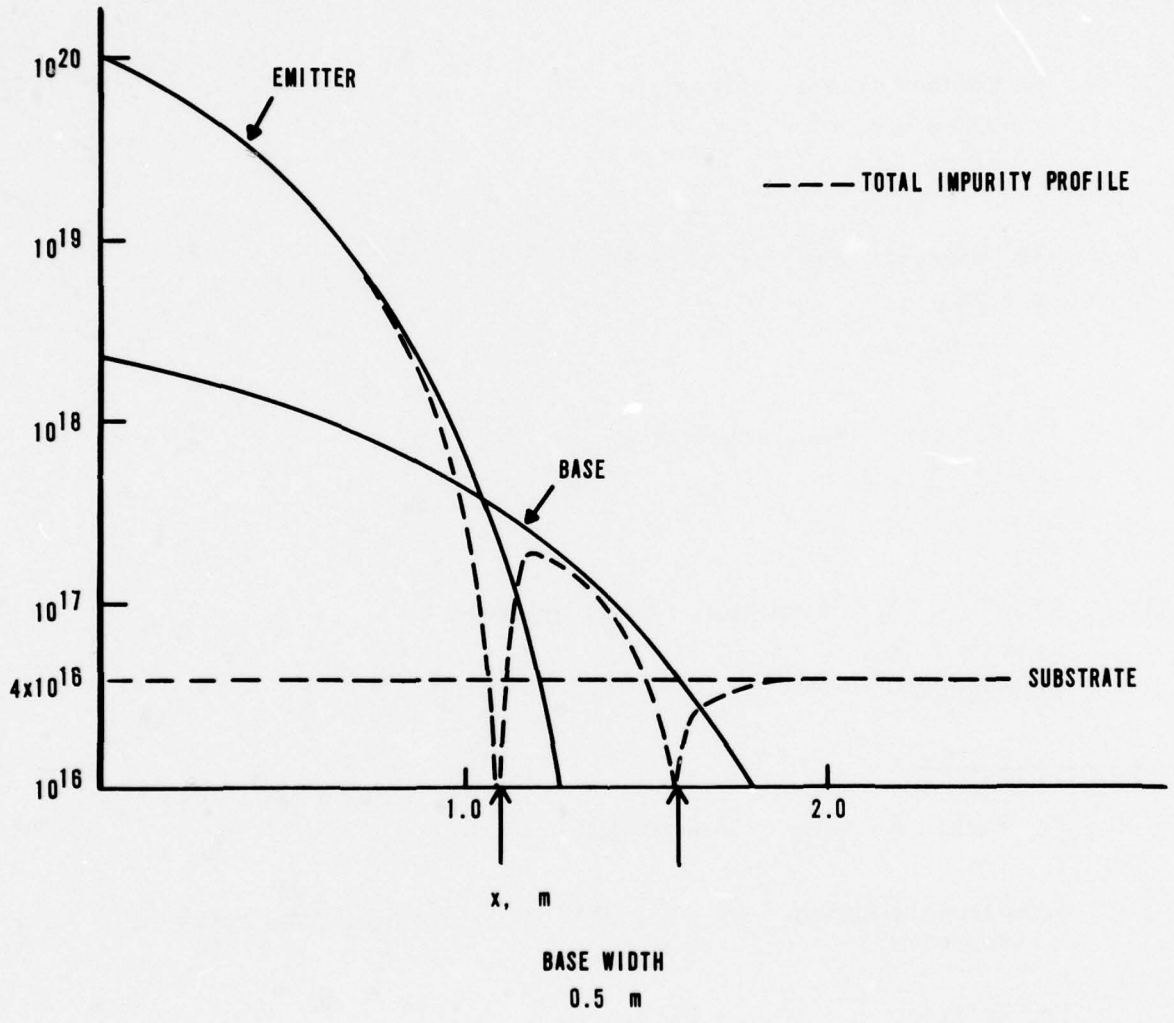


Figure 23. Doping Profile; Approximate Impurity Profiles Based on Gaussian Profiles Using Irvin's Curves. (These curves are hand-down fits through Cs and Xj points, so are merely representations of actual profiles.)

PACKAGED DEVICE PIN CONNECTIONS

Notation: Each can has a number scratched on the lid.

4A - Devices from wafer 4, chip A

[Chip A contains small transistor (structure #7) and emitter resistor (structure #15).]

4B - Devices from wafer 4, chip B

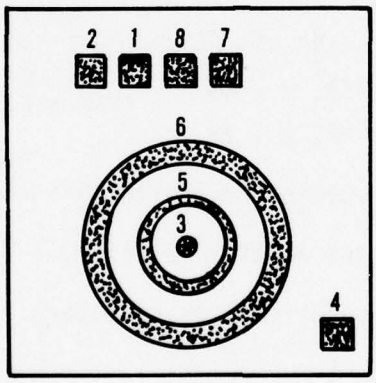
[Chip B contains structure #19, tetrode transistor.]

similarly for others such as

2A, 2B, 6A, 6B, etc. In each case the number refers to the wafer number. See process sequence.

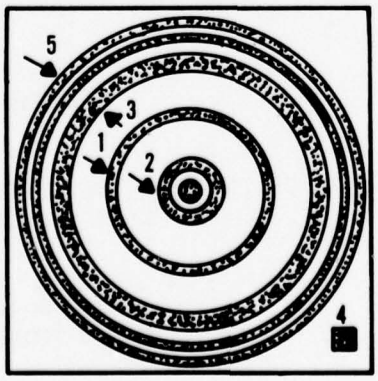
PIN CONNECTIONS

CHIP A



PIN 6 IS FIELD PLATE AT COLLECTOR-BASE JUNCTION

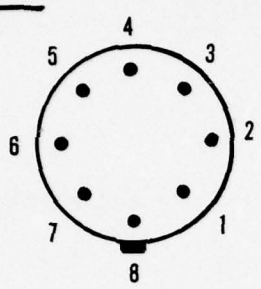
CHIP B



PIN 5 IS FIELD PLATE AT COLLECTOR BASE JUNCTION

PINS 3 & 2 ARE BASE CONTACTS

TO-5 HEADERS



Top View pin numbering.
Pin 4 is shorted to header, thus is used for collector.

Each can lid has number identifying wafer and type of chip contained therein.

Wafer numbers refer to processing sequence.

Wafer Numbers:
- 2 - ^{11}B emitter, $\beta \sim 40$
- 4 - ^{11}B emitter, $\beta \sim 75$
- 6 - ^{10}B emitter, $\beta \sim 40$
- 8 - ^{10}B emitter, $\beta \sim 75$
- 10 - 0.8 ^{11}B + 0.2 ^{10}B, $\beta \sim 40$
- 12 - 0.8 ^{11}B + 0.2 ^{10}B, $\beta \sim 75$

Note that β may vary somewhat from device to device.

Chip A: Small emitter transistor and emitter resistor.

Chip B: Tetrode transistor (base-under-emitter resistor).

PROCESS SEQUENCE FOR D0301A BIPOLAR TRANSISTORS

	Wafers are P-Boron (100) 0.4 - 0.6 Ω-cm NBS-2 Mask Set	12 Active 5 Controls
1.	Acid Clean	A + C
2.	Dry/Steam Oxide; 15/90 min, 1100° C	A + C
3.	Neg PR, lev 1 (base)	A
4.	BOE Etch	A + C
5.	Clean (PR strip)	A
6.	Phos Implant; 1.3×10^{14} at 160 keV	A + C
7.	Etch 4 min ($\sim$ 4000Å)	A + C
8.	Base drive-in, Dry O_2, 1100° C, 120 min	A + C
9.	Neg PR, lev 2 (emitter)	A
10.	Etch	A + C2-C5
11.	Boron Implant; $^{11}B + 5 \times 10^{15}$ at 60 keV	W 1-4, C2, C3
12.	Boron Implant; $^{10}B + 5 \times 10^{15}$ at 60 keV	W 5-8, C4
13.	Boron Implant; 80% ^{11}B + 20% ^{10}B + 5×10^{15}, 60 keV	W 9-12, C5
14.	Clean (PR strip)	A
15.	Deposit 5 x Å oxide	A + C
16.	Emitter drive-in; 1000° C, 30 min, N_2	A + C
17.	Emitter drive-in; 1000° C, 30 min, N_2	W3,4,7,8,11,12,C3
18.	Neg PR, lev 3 (contact)	A
19.	Etch	A + C
20.	Clean (PR strip)	A
21.	Probe wafer-gain measurement	
22.	Clean	
23.	Drive-in; 1100° C, 15 min, N_2	W1, 3
24.	30 sec Etch	W1, 3
25.	Probe wafer	
26.	Drive-in; 1100° C, 12 min, N_2	A + C except W1, 3
27.	15 sec Etch	A + C except W1, 3
28.	Probe wafer	
29.	Clean	A + C
30.	Drive-in; 1000° C, 30 min, N_2	A + C except W1, 3
31.	15 sec Etch	A + C except W1, 3
32.	Al Evap, 10KÅ	A
33.	Neg PR, lev 4 (metal)	A
34.	Etch Al	A
35.	PR strip	A
36.	Sinter, 5% forming gas, 450° C, 20 min	A
37.	Scribe, die attach, bond	

Notes: A means active wafers.
C means control wafers.

DEVICE NUMBER-- DU3010
DEVICE DESCRIPTION IS BIPOLAR TRANSISTOR AND WAS DEFINED 07/13/76
BY ANDERSON AND ENTERED BY TUCK
FOR 17 WAFERS
REMARKS WAFERS ARE P-BORON (100) 0.4-6.5; 12 ACTIVE + 5 CONTROLS; NBS/2 MASK SET

NEXT STEP OPN	NO	PROCESS NUMBER	DESCRIPTION	OPTR INIT	COMPLETION TIME	DATE	NUMBER WAFERS		NOTES
	1	1106CC	CLEAN	MRT	13:51	7/14/76	17		0
	2	3102HB	D/S OX 8000ACC	EH	15:58	7/14/76	17		17
	3	5100BB	747/60, LEV, L 3.55	MRT	9:50	7/15/76	12		0
	4	5111AH	ETCH HYPO + 1 MIN	MRT	10:10	7/15/76	17	*	0
	5	1100AA	CLEAN	DLW	11:24	7/15/76	17		0
	6	4134PV	PHOS IMP. A+C	REB	14: 1	7/15/76	17		0
	7	5111BB	ETCH 4 MIN	MRT	8:31	7/16/76	17		0
	8	3107EF	BASE DRIVEIN, A+C1,C	MRT	10:49	7/16/76	17		17
	9	5100EC	747/60, LEV.2, 3.58	MRT	16:14	7/16/76	12	*	0
	10	4505BH	BORON IMP,H+C,NOTE 1	REB	9:34	7/20/76	17		0
	11	1100AR	CLEAN	MRT	10:49	7/20/76	17	*	0
	12	2104AA	DEP.OX SKA,FRNTS A+C	MRT	15: 4	7/20/76	17		0
	13	3110EB	DRINEIN, A+C	MRT	9: 0	7/21/76	17		13
	14	3110EB	W3,4,7,8,11,12,C3	MRT	9:40	7/21/76	17		13
	15	5100AA	747/60, KEY 3,0.55	MRT	10:57	7/21/76	17		0
	16	5111AA	ETCH HPO(C1) A+C	MRT	12:47	7/21/76	17	*	0
	17	9999AA	HOLD, MODIFY ENG.	MRT	8:44	7/26/76	17		0
	18	1100AA	CLEAN	MRT	10:19	7/26/76	15		0
	19	3000NN	N2 ANNEAL 12M,1100C	MRT	10:54	7/26/76	17		0
	20	5111BD	30SEC ETCH	MRT	11:12	7/26/76	15		0
	21	9999AA	HOLD,NOTIFY ENG.	MRT	15:26	7/26/76	15	*	0
	22	1100BB	CLEAN	MRT	11:40	7/28/76	17		0
	23	6104BB	AL EVAP, 10KA	MRT	13:18	7/28/76	12		0
	24	5105RM	HR 100, LEV 4, 215	MRT	15:36	7/28/76	12		0
	25	5113RA	AL ETCH	MRT	16: 2	7/28/76	12		0
	26	1109AA	J100 RESIST STRIP	MRT	9: 2	7/29/76	12		0
	27	3100BB	SINTER,5K FRMING GAS	MRT	9:32	7/29/76	12		12
**	28	9000AA	MEAS RS,MJ ALL CONTROLS		:	/ /			
	29	9999AA	HOLD, NOTIFY ENG.		:	/ /			

SP REH
*- 1 NOTE 1: W1-4;C2,C3 IMPLANT B11 W5-8,C4 IMPLANT B10
*- 1 W9-12,C5 IMPLANT 20% B10, 60% B11
*- 1 ETCH LINE 9 MIN
*- 9 ETCH AFTER PR STEP A+02-05 CONTROLS HYPO + 1MIN
*- 11 WAFERS - TWO ACID CLEANS, HOT H2SO4, PLASMA STRIPPED (ACT. ONLY),SCRUB
*- 16 ETCH TIME 6MIN
*- 17 WAFERS #1,3, - 1100AA CLEAN, 1100 C H2 15 MIN (T9), 30S BOE - AFTER STE
*- 18 STEP #19 TUBE 9
*- 21 HI TER STEP 21 WAFERS (EXCP 1,3) SCRUBBED, ACID CLEAN AND ANNEALED T13,H2
*- 21 H2,1000 DEGREES C 30MIN
*- 26 SHT.RES 01:T-217; C-193; B-201; L-207; R-201 N TYPE
*- 26 C2: 1-24.3; C-24.0; B-23.9; L-24.8; R-24.8; P-TYPE;
*- 26 C3: C-24.6; C4: C-25.0; C5: C-25.3; P-TYPE RES. UNIFORM ACROSS WAFERS
*- 28 XJ C1 15519A C2/10538A C3/10916H C4/8999A C5/9271A CMB 7/29/76

APPENDIX F

TRANSISTOR CHARACTERISTICS

Table 4

DC GAIN MEASUREMENTS ON THE TEST TRANSISTORS
AVERAGE OF THREE DEVICES WITH STANDARD DEVIATION

I_c ma Device	.01	.02	.05	.1	.2	.5	1	2	10	20
2A	13.5	14.1	16.2	17.7	19.3	21.5	23.2	24.6	28.3	29.7
	1.35	1.97	2.06	2.19	2.24	2.39	2.28	2.34	2.31	1.70
4A	26.0	28.0	31.2	33.8	36.3	39.4	41.6	44.5	49.9	51.1
	5.05	4.88	4.95	4.93	5.41	5.39	5.37	5.19	5.38	5.21
6A	13.6	15.5	16.9	17.6	20.0	21.9	23.6	24.9	28.5	30.0
	1.22	1.62	1.29	1.41	1.46	1.23	1.17	1.23	1.47	1.59
8A	20.3	22.8	26.5	29.1	31.6	35.4	37.7	40.6	45.7	47.6
	2.51	2.24	2.17	2.12	1.97	1.53	1.73	1.68	2.00	1.60
10A	16.9	18.5	20.7	22.4	24.2	26.3	28.0	29.3	33.5	34.7
	1.30	1.15	1.26	1.11	1.16	1.16	1.50	1.29	1.44	1.32
12A	25.7	28.3	31.4	34.4	36.6	40.0	42.4	44.8	50.1	51.3
	5.08	4.89	4.85	5.49	5.20	5.34	5.51	5.46	5.91	5.95
2B							22.8	23.4	26.5	28.0
							2.92	2.05	1.32	1.17
4B							30.1	33.1	41.8	46.0
							4.58	3.67	6.93	.907
6B							22.7	24.6	29.9	32.3
							5.75	4.82	37.7	3.45
8B							41.9	39.4	43.5	47.0
							4.45	4.06	4.82	5.53
10B							19.8	21.7	26.5	28.5
							1.91	1.56	1.48	1.41
12B							29.2	32.3	40.8	45.0
							7.50	6.30	4.29	3.10

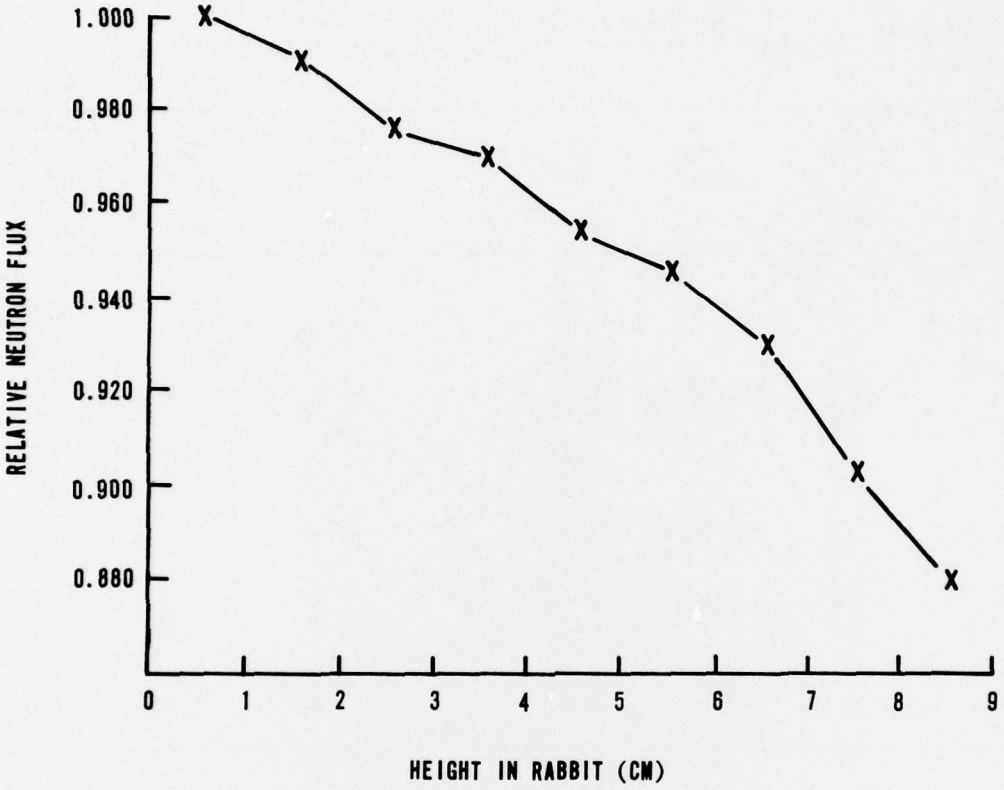
Table 5

LEAKAGES FOR TEST TRANSISTORS
AVERAGE OF THREE DEVICES AND STANDARD DEVIATION

Device	I_{CBO} 10VcB	I_{EBO} 3VBC	I_{CEO} 10Vce		I_{CBO} 10VcB	I_{EBO} 3VEE	I_{CEO} 10Vce
A	na	pa	μa	B	μa	na	μa
2	321	125	2.53	2	23.8	65.4	603
	141		1.21		8.46	110	260
4	415	19.5	3.25	4	12.5	8.27	544
	402	3.19	1.97		8.49	9.3	178
6	477	270	4.60	6	6.56	4.02	192
	240		2.45		3.69	4.06	147
8	122	26.4	3.12	8	8.00	2.5	675
	75	12.8	2.12		1.46	1.1	123
10	480	35	7.56	10	3.84	.556	134
	470		8.60		3.27	.306	113
12	156	222	3.26	12	1.21	2.21	295
	102	386	3.17		.402	1.53	103

APPENDIX G

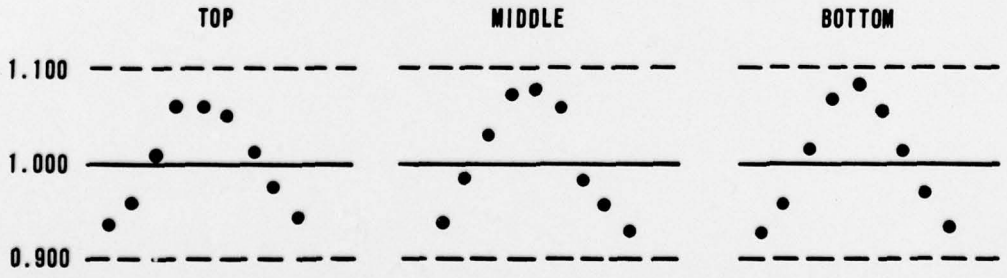
FLUX INFORMATION ON THERMAL COLUMN PNEUMATIC TUBE FACILITY (REF. 17)



Cu(Cd) RATIO = 3415 WITH CENTER GRAPHITE BLOCKS OUT

ABSOLUTE NEUTRON FLUX = 1.6×10^{11} $n \cdot cm^{-2} sec^{-1}$

CIRCUMFERENTIAL FLUX DISTRIBUTION



17. Becker, D. A., "Flux Information on Thermal Column Pneumatic Tube Facility," an unpublished data sheet available from the National Bureau of Standards, Reactor Operations Division, Gaithersburg, Maryland, June 1971.

APPENDIX H

DERIVATION OF THE RELATIVE DAMAGE EQUATION

One measure of relative effectiveness of thermal neutrons to fast neutrons in producing damage in transistors would be the ratio of the thermal neutrons bulk damage constant to the fast-neutron bulk damage constant. Recall the bulk damage equation

$$\Delta(1/\beta) = C\Phi$$

Since $\Delta(1/\beta)$ is a measure of the lattice defects (Recombination Centers) in the base region, C, the bulk damage constant, must be a measure of the defects produced in the base region per neutron.

Recall that the number of reactions that occur as a result of a fast-neutron irradiation is

$$R = \Sigma \Phi V$$

where R is the reactions, Σ is the macroscopic cross section, Φ is the neutron fluence, and V is the volume in which the reactions occur. Recall also that the macroscopic cross section is given by

$$\Sigma = N \sigma$$

where N is the atom density and σ is the microscopic cross section. Thus, it can be seen that the number of 1 MeV neutron reactions that occur in the base region of a transistor would be

$$R = \sigma_{1\ MeV\ Si}\ N_{si}\ \Phi\ V$$

Define $u_{1\ MeV}$ as the defects per fast neutron (1 MeV); then the fast-neutron bulk damage constant would be given by

$$C_{1\ MeV} = u_{1MeV}\sigma_{1\ MeVSi}\ N_{si} V_{base}$$

For the thermal neutron case, the neutron reactions take place in the emitter region, while the gain degrading damage is done by the lithium nucleus and the alpha particle in the base region. The geometry factor (G) derived in appendix B gives the particles doing damage in the base region per reaction in the emitter region. Thus, the thermal neutron bulk damage constant would be given by

$$C_{thermal} = \left(U_{\alpha} G_{\alpha} + U_{Li}\ G_{Li}\right) \sigma_{thermB10} N_{B10} V_{Emitter}$$

As long as the combined width of the emitter region and the base region is less than the path length of the lithium recoil, G_{α} and G_{Li} should remain in the same ratio. For this case it should be possible to factor out from the quantity in parenthesis an average number of defects per particle (alpha or lithium). Calling this average $U_{thermal}$, it follows that

$$C_{thermal} = U_{thermal} \left(G_{\alpha} + G_{Li}\right) \sigma_{thermB10} N_{B10} V_{Emitter}$$

and

$$\frac{C_{thermal}}{C_{1MeV}} = \frac{U_{thermal} \left(G_{\alpha} + G_{Li}\right) \sigma_{thermB10} N_{B10} V_{Emitter}}{U_{1MeV} \quad \sigma_{1MeV} \quad N_{si} \quad V_{base}}$$

$\frac{U_{thermal}}{U_{1MeV}}$ was experimentally found to be approximately 1/3.3 or 0.30 as is indicated in section IV. Also, since the areas of the base and the emitter are equal, the areas would divide out of the relative damage equation. The result is

$$\frac{C_{thermal}}{C_{1MeV}} = \frac{0.3 \left(G_{\alpha} + G_{Li}\right) \sigma_{thermB10} N_{B10} W_{Emitter}}{\sigma_{1MeVSi} \quad N_{si} \quad W_{base}}$$

where W is the width of the region.

DISTRIBUTION LIST

DEPARTMENT OF DEFENSE

Defense Communication Engineer Center
ATTN: Code R410, James W. McLean
ATTN: Code R320, C. W. Bergman

Director
Defense Communications Agency
ATTN: Code 930, Monte I. Burgett, Jr.
ATTN: Code 540.5
ATTN: Code 430

Defense Documentation Center
Cameron Station
12 cy ATTN: TC

Commander
Defense Electronic Supply Center
ATTN: ECS, Joe W. Dennis

Director
Defense Intelligence Agency
ATTN: DB-4C, Edward O'Farrell
ATTN: DS-4A2

Director
Defense Nuclear Agency
ATTN: DDST
ATTN: RAEV
ATTN: STVL
2 cy ATTN: STVL, LTC W. Adams
3 cy ATTN: TITL, Tech. Library

Dir. of Defense Rsch. & Engineering
ATTN: S&SS (OS)

Commander, Field Command
Defense Nuclear Agency
ATTN: FCPR

Director
Interservice Nuclear Weapons School
ATTN: Document Control

Director
Joint Strat. Tgt. Planning Staff, JCS
ATTN: JLTW-2

Chief
Livermore Division, Field Command, DNA
Lawrence Livermore Laboratory
ATTN: FCPRL

Director
National Security Agency
ATTN: Orlando O. Van Gunten, R-425

OJCS/J-3
ATTN: J-3, RDTA Br., WWMCCS, Plans Div.

DEPARTMENT OF THE ARMY

Project Manager
Army Tactical Data Systems
U.S. Army Electronics Command
ATTN: Dwaine B. Huewe
ATTN: DRCPN-TDS-SD

DEPARTMENT OF THE ARMY (Continued)

Commander
BMD System Command
ATTN: BDMSC-TEN, Noah J. Hurst

Chief C-E Services Division
U.S. Army Communications Cmd.
ATTN: CEEO-7, Wesley T. Heath, Jr.

Commander
Frankford Arsenal
ATTN: SARFA-FCD, Marvin Elnick

Commander
Harry Diamond Laboratories
ATTN: DRXDO-RBH, Paul A. Caldwell
ATTN: DRXDO-EM, Robert E. McCoskey
ATTN: DRXDO-TI, Tech. Lib.
ATTN: DRXDO-RC, Robert B. Oswald, Jr.
ATTN: J. Halpin
ATTN: DRXDO-EM, R. Bostak
ATTN: J. McGarrity
ATTN: DRXDO-RB, Joseph R. Miletta
ATTN: DRXDO-NP, Francis N. Wimenitz
ATTN: DRXDO-EM, J. W. Beilfuss
ATTN: DRXDO-TR, Edward E. Conrad
ATTN: DRXDO-RCC, John A. Rosado

Commanding Officer
Night Vision Laboratory
ATTN: CPT Allan S. Parker

Commander
Picatinny Arsenal
ATTN: SARPA-ND-N
ATTN: SARPA-TS-I-E, Abraham Grinoch
ATTN: SMUPA-ND-D-B, Edward J. Arber
ATTN: SMUPA-ND-N-E
ATTN: SMUPA-ND-W

Commander
Redstone Scientific Information Ctr.
U.S. Army Missile Command
3 cy ATTN: Chief, Documents

Secretary of the Army
ATTN: ODUSA or Daniel Willard

Director
TRASANA
ATTN: ATAA-EAC, Francis N. Wenaas

Director
U.S. Army Ballistic Research Labs.
ATTN: DRXBR-X, Julius J. Meszaros
ATTN: DRXBR-VL, John W. Kinch
ATTN: DRXBR-VL, Robert L. Harrison

Commander
U.S. Army Communications Cmd.
ATTN: ACC-FD-M, Lawrence E. Cork

Chief
U.S. Army Communications Sys. Agency
ATTN: SCCM-AD-SV, Library

DEPARTMENT OF THE ARMY (Continued)

Commander
U.S. Army Electronics Command
ATTN: DRSEL-PL-ENV, Hans A. Bomke
ATTN: DRSEL-CE, T. Preiffer
ATTN: DRSEL-TL-IR, Edwin T. Hunter
ATTN: DRSEL-CT-HDK, Abraham E. Cohen
ATTN: DRSEL-GG-TD, W. R. Werk
ATTN: DRSEL-NL-D

Commandant
U.S. Army Engineer School
ATTN: ATSE-CTD-CS, C. S. Grazier

Commander in Cnief
U.S. Army Eurpose and Seventh Army
ATTN: ODCSE-E, AEAGE-PI

Commandant
U.S. Army Field Artillery School
ATTN: ATSFA-CTD-ME, Harley Moberg

Commander
U.S. Army Materiel Dev. & Readiness Cmd.
ATTN: DRCDE-D, Lawrence Flynn

Commander
U.S. Army Missile Command
ATTN: DRCPM-PE-EA, Wallace O. Wagner
ATTN: DRCPM-LCEX, Howard H. Henriksen
ATTN: DRSMI-RGD, Vic Ruwe

Commander
U.S. Army Mobility Equip. R&D Ctr.
ATTN: AMSEL-NV-SD, J. H. Carter
ATTN: STSFB-MW, John W. Bond, Jr.

Chief
U.S. Army Nuc. and Chemical Surety Gp.
ATTN: MOSG-ND, Maj Sidney W. Winslow

Commander
U.S. Army Nuclear Agency
ATTN: ATCN-W, LTC Leonard A. Sluga

Commander
U.S. Army Security Agency
ATTN: IARD-T, Robert H. Burkhardt

Commander
U.S. Army Tank Automotive Command
ATTN: DRCPM-GCM-SW, Lyle A. Wolcott
ATTN: DRSTA-RHM, 1LT Peter A. Hasek

Commander
U.S. Army Test & Evaluation Comd.
ATTN: DRSTE-NB, Russel R. Galasso
ATTN: DRSTE-EL, Richard I. Kolchin

Commander
U.S. Army Training & Doctrine Comd.
ATTN: ATORI-OP-SD

Commander
White Sands Missile Range
ATTN: STEWS-TE-NT, Marvin P. Squires

DEPARTMENT OF THE NAVY

Chief of Naval Research
ATTN: Code 427

DEPARTMENT OF THE NAVY (Continued)

Commanding Officer
Naval Avionics Facility
ATTN: Branch 942, D. J. Repass

Commander
Naval Electronic Systems Command
Naval Electronic Systems Cmd, Hqs.
ATTN: Code 504511, Charles R. Suman
ATTN: Code 50451
ATTN: PME 117-21
ATTN: Elex. 05323, Cleveland F. Watkins
ATTN: Code 5032, Charles W. Neill

Director
Naval Research Laboratory
ATTN: Code 2627, Doris R. Folen
ATTN: Code 4104, Emanual L. Brancato
ATTN: Code 7701, Jack D. Brown
ATTN: Code 5216, Harold L. Hughes
ATTN: Code 6601, E. Wolicki
ATTN: Code 6631, James C. Ritter
ATTN: Code 5210, John E. Davey
ATTN: Code 6440, George Sigel

Commander
Naval Sea Systems Command
ATTN: SEA-9931, Riley B. Lane
ATTN: SEA-9931, Samuel A. Barham

Commander
Naval Ship Engineering Center
ATTN: Code 6174D2, Edward F. Duffy

Officer-in-Charge
Naval Surface Weapons Center
ATTN: Code 431, Edwin B. Dean
ATTN: Code WA52, R. A. Smith
ATTN: Code WA501, Navy Nuc. Prgms. Off.
ATTN: Code WA50

Commander
Naval Weapons Center
ATTN: Code 533, Tech. Lib.

Commanding Officer
Naval Weapons Evaluation Facility
ATTN: Code ATG, Mr. Stanley

Commanding Officer
Naval Weapons Support Center
ATTN: Code 70242, Joseph A. Munarin
ATTN: Code 7024, James Ramsey

Director
Strategic Systems Project Office
ATTN: SP-2701, John W. Pitsenberger
ATTN: NSP-27331, Phil Spector
ATTN: NSP-230, David Gold
ATTN: NSP-2342, Richard L. Coleman

DEPARTMENT OF THE AIR FORCE

AF Aero-Propulsion Laboratory, AFSC
ATTN: POE-2, Joseph F. Wise

AF Institute of Technology, AU
ATTN: ENP, Charles J. Bridgman

DEPARTMENT OF THE AIR FORCE (Continued)

AF Weapons Laboratory, AFSC
ATTN: ELC
ATTN: ELA
ATTN: ELXT
ATTN: ELS
ATTN: NTS
ATTN: DEX
ATTN: HO, Dr. Minge
2 cy ATTN: SUL
5 cy ATTN: ELP, Maj Chronister

AFTAC
ATTN: TFS, Maj Marion F. Schneider

Air Force Avionics Laboratory, AFSC
ATTN: DHE, H. J. Hennecke
ATTN: DHM, C. Friend
ATTN: DH, Lt Col McKenzie
ATTN: AAT, Mason Friar

AUL (LDE)
ATTN: LDE

Commander
ASD
ATTN: ASD-YH-EX, Lt Col Robert Leverette
ATTN: ENACC, Robert L. Fish

Headquarters
Electronic Systems Division/DC
ATTN: DCKE, Lewis Staples

Headquarters
Electronic Systems Division/YS
ATTN: YSEV

Headquarters
Electronic Systems Division/YW
ATTN: YWEI

Commander
Foreign Technology Division, AFSC
ATTN: ETD/PDJC
ATTN: ETDP

Commander
Rome Air Development Center, AFSC
ATTN: RBRAC, I. L. Krulac
ATTN: RBRP, Clyde Lane

Commander
Rome Air Development Center, AFSC
ATTN: ETS, R Dolan
ATTN: ETS, A. Kahan
ATTN: ET, R. Buchanan

SAMSO/DY
ATTN: DYS, Maj Larry A. Darda

SAMSO/IN
ATTN: IND, I. J. Judy

SAMSO/MN
ATTN: MNNH
ATTN: MNNG
ATTN: MNNG, Capt David J. Strobel

DEPARTMENT OF THE AIR FORCE (Continued)

SAMSO/RS
ATTN: RSMG
ATTN: RSSE

SAMSO/SK
ATTN: SKF

SAMSO/SZ
ATTN: SZJ

Commander in Chief
Strategic Air Command
ATTN: XPFS, Capt Deraad
ATTN: NRI-Stinfo Library

DEPARTMENT OF ENERGY

University of California
Lawrence Livermore Laboratory
ATTN: Joseph E. Keller, Jr., L-125
ATTN: Hans Kruger, L-96 (Class L-94)
ATTN: Tech. Info. Dept. L-3
ATTN: Lawrence Cleland, L-156
ATTN: Donald J. Meeker, L-545 (Class L-153)

Los Alamos Scientific Laboratory
ATTN: Doc. Con. for J. Arthur Freed
ATTN: Doc. Con. for Bruce W. Noel

Sandia Laboratories
ATTN: Doc. Con. for Org. 1933, F. N. Coppage
ATTN: Doc. Con. for Org. 2110, J. A. Hood
ATTN: Doc. Con. for Org. 2140, R. Gregory
ATTN: Doc. Con. for 3141, Sandia Rpt. Coll.

Department of Energy
Albuquerque Operations Office
ATTN: Document Control for WSSB

OTHER GOVERNMENT AGENCY

Department of Commerce
National Bureau of Standards
ATTN: Judson C. French

DEPARTMENT OF DEFENSE CONTRACTORS

Aerojet Electro-Systems Co.
Div. of Aerojet-General Corporation
ATTN: Thomas D. Hanscome

Aerospace Corporation
ATTN: J. Benveniste
ATTN: Irving M. Garfunkel
ATTN: John Ditre
ATTN: Julian Reinheimer
ATTN: Library
ATTN: S. P. Bower

Analog Technology Corporation
ATTN: John Joseph Baum

Avco Research & Systems Group
ATTN: Research Lib. A830, Rm. 7201

The BDM Corporation
ATTN: T. H. Neighbors

DEPARTMENT OF DEFENSE CONTRACTORS (Continued)

The BDM Corporation
ATTN: D. R. Alexander

The Bendix Corporation
Communication Division
ATTN: Document Control

The Bendix Corporation
Research Laboratories Division
ATTN: Max Frank
ATTN: Mgr. Prgm. Dev., Donald J. Niehaus

The Bendix Corporation
Navigation and Control Group
ATTN: George Gartner

The Boeing Company
ATTN: Howard W. Wicklein, MS 17-11
ATTN: Itsu Amura, 2R-00
ATTN: Aerospace Library
ATTN: Robert S. Caldwell, 2R-00
ATTN: Carl Rosenberger, 2R-00

Booz-Allen and Hamilton, Inc.
ATTN: Raymond J. Chrisner

Brown Engineering Company, Inc.
ATTN: John M. McSwain, MS 18

Burroughs Corporation
Federal and Special Systems Group
ATTN: S. E. Gluck

California Institute of Technology
Jet Propulsion Laboratory
ATTN: J. Bryden
ATTN: A. G. Stanley

Charles Stark Draper Laboratory, Inc.
ATTN: Paul R. Kelly
ATTN: Kenneth Fertig

Cincinnati Electronics Corporation
ATTN: C. R. Stump

Computer Sciences Corporation
ATTN: Richard H. Dickhaut

Control Data Corporation
ATTN: Jack Meehan

Cutler-Hammer, Inc.
AIL Division
ATTN: Central Tech. Files, Anne Anthony

University of Denver
Colorado Seminary
Denver Research Institute
ATTN: Sec. Officer for Fred P. Venditti

Dikewood Industries, Inc.
ATTN: L. Wayne Davis

E-Systems, Inc.
Greenville Division
ATTN: Library 8-50100

Effects Technology, Inc.
ATTN: Edward John Steele

DEPARTMENT OF DEFENSE CONTRACTORS (Continued)

Fairchild Camera and Instrument Corp.
ATTN: Sec. Dept. for 2-233, David K. Myers

Fairchild Industries, Inc.
Sherman Fairchild Technology Center
ATTN: Mgr. Config. Data & Standards

Ford Aerospace & Communications Corp.
ATTN: Samuel R. Crawford, MS 531
ATTN: Edward R. Hahn, MX-X22
ATTN: Donald R. McMorrow, MS G30

Ford Aerospace & Communications Operations
ATTN: Tech. Info. Section
ATTN: Ken C. Attinger
ATTN: E. R. Poncelet, Jr.

The Franklin Institute
ATTN: Ramie H. Thompson

Garrett Corporation
ATTN: Robert E. Weir, Dept. 93-9

General Dynamics Corp.
Electronics Div., Orlando Operations
ATTN: D. W. Coleman

General Electric Company
Space Division
ATTN: John L. Andrews
ATTN: Joseph C. Peden, VFSC, Rm. 4230M
ATTN: Larry I. Chasen

General Electric Company
Re-Entry & Environmental Systems Div.
ATTN: Robert V. Benedict
ATTN: John W. Palchefsky, Jr.

General Electric Company
Ordnance Systems
ATTN: Joseph J. Reidl

General Electric Company
TEMPO-Center for Advanced Studies
ATTN: DASIAC
ATTN: M. Espig
ATTN: Royden R. Rutherford

General Electric Company
Aircraft Engine Business Group
ATTN: John A. Ellerhorst, E 2

General Electric Company
Aerospace Electronics Systems
ATTN: Charles M. Hewison, Drop 624
ATTN: W. J. Patterson, Drop 233

General Electric Company
ATTN: David W. Pepin, Drop 160

General Electric Company-TEMPO
ATTN: DASIAC for William Alfonte

General Research Corporation
ATTN: Robert D. Hill

Georgia Institute of Technology
Georgia Tech. Research Institute
ATTN: R. Curry

DEPARTMENT OF DEFENSE CONTRACTORS (Continued)

Georgia Institute of Technology
Office of Contract Administration
ATTN: Res. & Sec. Coord. for Hugh Denny

Grumman Aerospace Corporation
ATTN: Jerry Rogers, Dept. 533

GTE Sylvania, Inc.
Electronics Systems Grp-Eastern Div.
ATTN: Charles A. Thornhill, Librarian
ATTN: James A. Waldon
ATTN: Leonard L. Blaisdell

GTE Sylvania, Inc.
ATTN: H&V Group
ATTN: Paul B. Fredrickson
ATTN: Charles H. Ramsbottom
ATTN: Herbert A. Ullman

Gulton Industries, Inc.
Engineered Magnetics Division
ATTN: Engn. Magnetics Div.

Harris Corporation
Harris SemiConductor Division
ATTN: Wayne E. Abare, MS 16-111
ATTN: T. L. Clark, MS 4040
ATTN: Carl F. Davis, MS 17-220

Hazeltine Corporation
ATTN: Tech. Info. Ctr., M. Waite

Honeywell Incorporated
Avionics Division
ATTN: Ronald R. Johnson, A1622
ATTN: R. J. Kell, MS S2572

Honeywell Incorporated
Avionics Division
ATTN: MS 725-J, Stacey H. Graff
ATTN: MS 725-5A, Harrison H. Noble

Honeywell Incorporated
Radiation Center
ATTN: Technical Library

Hughes Aircraft Company
ATTN: Kenneth R. Walker, MS D157
ATTN: John B. Singletary, MS 6-D133
ATTN: Billy W. Campbell, MS 6-E-110

Hughes Aircraft Company, El Segundo Site
ATTN: William W. Scott, MS A1080
ATTN: Edward C. Smith, MS A620

IBM Corporation
ATTN: Frank Frankovsky

IIT Research Institute
ATTN: Irving N. Mindel

Int. Tel. & Telegraph Corporation
ATTN: Alexander T. Richardson

ION Physics Corporation
ATTN: Robert D. Evans

DEPARTMENT OF DEFENSE CONTRACTORS (Continued)

IRT Corporation
ATTN: R. L. Mertz
ATTN: MDC
ATTN: Ralph H. Stahl
ATTN: Leo D. Cotter

Jaycor
ATTN: Catherine Turesko
ATTN: Robert Sullivan

Johns Hopkins University
Applied Physics Laboratory
ATTN: Peter E. Partridge

Kaman Sciences Corporation
ATTN: W. Foster Rich
ATTN: Walter E. Ware
ATTN: Jerry I. Lubell
ATTN: Donald H. Bryce
ATTN: Albert P. Bridges

Litton Systems, Inc.
Guidance & Control Systems Division
ATTN: Val J. Ashby, MS 67
ATTN: John P. Retzler

Lockheed Missiles & Space Co., Inc.
ATTN: George F. Heath, D/81-14
ATTN: Edwin A. Smith, Dept. 85-85
ATTN: Benjamin T. Kimura, Dept. 81-14
ATTN: L. Rossi, Dept. 81-64
ATTN: Samuel I. Taimuty, Dept. 85-85

Lockheed Missiles & Space Co., Inc.
ATTN: Tech. Info. Ctr. D/Coll.

MIT Lincoln Laboratory
ATTN: Leona Loughlin, Librarian, A-082

Martin Marietta Aerospace
Orlando Division
ATTN: William W. Mras, MP-413
ATTN: Jack M. Ashford, MP-537
ATTN: Mona C. Griffith, Lib. MP-30

Martin Marietta Corporation
Denver Division
ATTN: Paul G. Kase, Mail 8203
ATTN: Research Lib. 6617, Jay R. McKee
ATTN: J. E. Goodwin, Mail 0452

McDonnell Douglas Corporation
ATTN: Tom Ender
ATTN: Technical Library

McDonnell Douglas Corporation
ATTN: Stanley Schneider

McDonnell Douglas Corporation
ATTN: Technical Library, C1-290/36-84

Mission Research Corporation
ATTN: William C. Hart

Mission Research Corporation
ATTN: David E. Merewether

Mission Research Corporation-San Diego
ATTN: J. P. Raymond
ATTN: V. A. J. Van Lint

DEPARTMENT OF DEFENSE CONTRACTORS (Continued)

The Mitre Corporation
ATTN: M. E. Fitzgerald

National Academy of Sciences
ATTN: National Materials Advisory Board for R. S. Shane

University of New Mexico
Electrical Engineering & Computer Science Dept.
ATTN: Harold Southward

Northrop Corporation
Electronic Division
ATTN: Boyce T. Ahlport

Northrop Corporation
Northrop Research & Technology Ctr.
ATTN: J. R. Srour
ATTN: Orlie L. Curtis, Jr.
ATTN: David N. Pocock

Northrop Corporation
Electronic Division
ATTN: John M. Reynolds
ATTN: Vincent R. DeMartino
ATTN: Joseph D. Russo

Palisades Inst. for Rsch. Services, Inc.
ATTN: Records Supervisor

Physics International Company
ATTN: Doc. Con. for Charles H. Stallings
ATTN: Doc. Con. for John H. Huntington

R&D Associates
ATTN: S. Clay Rogers
ATTN: William R. Graham, Jr.

Raytheon Company
ATTN: Gajanan H. Joshi, Radar Sys. Lab.

Raytheon Company
ATTN: Harold L. Flescher

RCA Corporation
Government Systems Division
Astro Electronics
ATTN: George J. Brucker

RCA Corporation
David Sarnoff Research Center
ATTN: K. H. Zaininger

RCA Corporation
Camden Complex
ATTN: E. Van Keuren, 13-5-2

Research Triangle Institute
ATTN: Eng. Div., Mayrant Simons, Jr.

Rockwell International Corporation
ATTN: Donald J. Stevens, FA70
ATTN: K. F. Hull
ATTN: James E. Bell, HA10
ATTN: N. J. Rudie, FA53
ATTN: George C. Messenger, FB61
ATTN: L. Apodaca, FA53

DEPARTMENT OF DEFENSE CONTRACTORS (Continued)

Rockwell International Corporation
ATTN: T. B. Yates

Rockwell International Corporation
Collins Division
ATTN: Dennis Sutherland
ATTN: Mildred A. Blair
ATTN: Alan A. Langenfeld

Sanders Associates, Inc.
ATTN: Moe L. Aitel, NCA 1-3236

Science Applications, Inc.
ATTN: Larry Scott
ATTN: J. Robert Beyster

Science Applications, Inc.
ATTN: J. Roger Hill

Simulation Physics, Inc.
ATTN: Roger G. Little

The Singer Company (Data Systems)
ATTN: Tech. Info. Center

Sperry Flight Systems Division
Sperry Rand Corporation
ATTN: D. Andrew Schow

Sperry Rand Corporation
Sperry Division
ATTN: Charles L. Craig, EV
ATTN: Paul Maraffino

Sperry Univac
ATTN: James A. Inda, MS 41T25

Stanford Research Institute
ATTN: Philip J. Dolan

Stanford Research Institute
ATTN: MacPherson Morgan

Sundstrand Corporation
ATTN: Curtis B. White

Systron-Donner Corporation
ATTN: Gordon B. Dean
ATTN: Harold D. Morris

Texas Instruments, Inc.
ATTN: Donald J. Manus, MS 72

TRW Defense & Space Sys. Group
ATTN: Robert M. Webb, R1-2410
ATTN: H. H. Holloway, R1-2036
ATTN: Tech. Info. Center/S-1930
2 cy ATTN: O. E. Adams, R1-1144
2 cy ATTN: R. K. Plebuch, R1-2078

TRW Defense & Space Sys. Group
San Bernardino Operations
ATTN: R. Kitter
ATTN: F. B. Fay

TRW Systems Group
ATTN: Donald W. Pugsley

DEPARTMENT OF DEFENSE CONTRACTORS (Continued)

United Technologies Corporation
Hamilton Standard Division
ATTN: Raymond G. Giguere

Vought Corporation
ATTN: Technical Data Ctr.

DEPARTMENT OF DEFENSE CONTRACTORS (Continued)

Vought Corporation
Michigan Division
ATTN: Tech. Lib.

Westinghouse Electric Corporation
Defense & Electronics Systems Ctr.
ATTN: Henry P. Kalapaca, MS 3525